A reliable new three-dimensional potential energy surface for H_2–Kr

Hua Wei and Robert J. Le Roy[a)]
Guelph-Waterloo Center for Graduate Work in Chemistry and Biochemistry, University of Waterloo, Waterloo, Ontario N2L 3G1, Canada

Richard Wheatley[b)] and William J. Meath[c)]
Department of Chemistry, University of Western Ontario, London, Ontario N6A 3B7, Canada

(Received 12 October 2004; accepted 30 November 2004; published online 22 February 2005)

An improved three-dimensional potential energy surface for the H_2–Kr system is determined from a direct fit of new infrared spectroscopic data for H_2–Kr and D_2–Kr to a potential energy function form based on the exchange-Coulomb model for the intermolecular interaction energy. These fits require repetitive, highly accurate simulations of the observed spectra, and both the strength of the potential energy anisotropy and the accuracy of the new data make the "secular equation perturbation theory" method used in previous analyses of H_2–(rare gas) spectra inadequate for the present work. To address this problem, an extended version of the "iterative secular equation" method was developed which implements direct Hellmann–Feynman theorem calculation of the partial derivatives of eigenvalues with respect to parameters of the Hamiltonian which are required for the fits. © *2005 American Institute of Physics*. [DOI: 10.1063/1.1850462]

I. INTRODUCTION

For over a quarter century molecular hydrogen–{rare gas} (H_2–Rg) van der Waals molecules have been leading prototype systems with regard to the determination of accurate multidimensional potential energy surfaces from experimental data.[1–7] Very high quality potentials have also been determined for more strongly bound and/or more rigid systems such as Ar–HF,[8] Ar–HCl,[9] He–CO,[10–13] Ar–CO_2,[14] Ne–HF,[15] $(HF)_2$,[16] and $(HCl)_2$.[17] The detail and accuracy of these surfaces have helped stimulate the development of better theoretical methods for the *ab initio* calculation of van der Waals interactions, which in most favorable cases are now beginning to approach spectroscopic accuracy in the potential well region.[18–20] In the H_2–Rg family, most attention to date has been focused on the H_2–Ar system for which the widest range of spectroscopic,[7,21–24] collisional,[25–28] and bulk property data[29–33] are available. However, the heavier H_2–Kr and H_2–Xe species are also interesting for a number of reasons. (i) The presence of larger numbers of electrons make them more challenging test systems for *ab initio* methods of calculating van der Waals interactions. (ii) Their stronger isotropic and anisotropic interactions make accurate quantal calculation of vibration-rotation eigenvalues of these systems distinctly more challenging than for H_2–Ar, a fact which stimulated our development of a better method for performing such calculations. (iii) Since the hydrogen–{rare gas} complexes are the only atom-diatom species for which the dependence of the potential energy on diatom bond length has been quantitatively determined from experiment,[1–7] having the best possible three-dimensional surfaces for the whole family of systems should prove useful in understanding trends in such behavior and allowing quantitative tests of models for vibrational inelasticity.

The first reported three-dimensional potential energy surface for H_2–Kr was obtained[1] from an empirical fit to the 1971 infrared (IR) data of McKellar and Welsh.[21] While remarkable for its time, the resolution of those measurements was substantially lower than that of data available today.[34] Moreover, that surface was defined using simple empirical Lennard–Jones(12,6) functions for the radial behavior of the various components of the potential.[1] Subsequent reanalyses of those same data used increasingly sophisticated potential function models which incorporated both the correct theoretically known long-range behavior[3] and a "collapsed-diatom limit" constraint which allowed a more realistic overall diatom-stretching dependence to be determined.[5,35] However, the fact that the quality of agreement with experiment obtained using these three different models for the potential was essentially the same illustrates the fact that the available data[21] were not particularly sensitive to the radial shape of the potential energy surface. This conclusion was not surprising, since the zero-point energy of H_2–Kr is approximately half of the well depth and the observed transitions only involve rotational sublevels of the lowest vibrational stretching level of the van der Waals bond. This observation underlines the importance of using a physically realistic model for the potential surface when fitting to experimental data of this type.

The best previous potential energy surface for H_2–Kr is the semiempirical (some parameters being fixed from theory) "TT_3" function of Ref. 6. It was determined from a fit to a combination of the somewhat more accurate (estimated uncertainties[23] ≈0.02 vs 0.03 cm^{-1} for the data of Ref. 21) IR H_2–Kr data of Ref. 23 and the lower resolution D_2–Kr

[a)]Electronic mail: leroy@UWaterloo.ca
[b)]Present address: Department of Chemistry, University of Nottingham, Nottingham NG7 2RD, UK.
[c)]Also at the Centre for Interdisciplinary Studies in Chemical Physics, University of Western Ontario, London, Ontario N6A 3B7, Canada.

IR data from Ref. 21 plus the one reported hyperfine transition energy.[22] This TT_3 model for the potential energy function is quite similar to the "$BC_3(6,8)$" model of Ref. 35 (as reported in Ref. 5), but utilizes a more sophisticated representation of the long-range part of the potential. While qualitatively quite similar to previous potential energy surfaces for this system, the fact that the TT_3 surface accurately reproduces the hyperfine datum,[22] for which the earlier surfaces gave very poor predictions,[6] indicated that its potential anisotropy for complexes formed with ground state ($v=0$) H_2 was substantially better than that of the earlier surfaces. Moreover, that analysis was the first to discern a measurable contribution of the $P_4(\cos\theta)$ potential anisotropy for any of the H_2-Rg systems.

McKellar has now obtained a new body of infrared and far-infrared data for H_2-Kr and D_2-Kr which is more extensive and substantially more accurate (estimated uncertainties ± 0.004 cm^{-1}) than the data available previously.[34] The main objective of the present work is to utilize these extensive new high resolution IR data and the hyperfine datum of Waaijer and Reuss[22] to determine the best possible three-dimensional potential energy surface for this system. The substantially greater accuracy and extent of these new IR data[34] means that the resulting potential surface should be more precise and reliable that those reported heretofore.[1,3,5,6] Experimental second virial[36] and diffusion[37] coefficients are used to provide an independent assessment of the quality of the new potential energy surface.

To date, no full *ab initio* potential energy surfaces have been reported for H_2-Kr. This is not surprising since the large numbers of electrons involved would challenge even the best "supermolecule"-type electronic structure programs of today. However, for interactions between closed-shell species remarkably successful methods have been developed which are based on a partitioning of the interaction energy into a number of components which can be estimated fairly accurately at relatively low levels of computational effort.[7,11,38–58] A potential function of this type is the basis of the present analysis.

A least-squares fitting scheme for refining a trial potential energy surface typically requires many iterative cycles, in each of which the entire spectrum must be computed to "spectroscopic accuracy" and accurate partial derivatives of each datum with respect to each fitting parameter must be determined. Our latest study of the H_2-Ar system[7] and previous analyses[6] for H_2-Ar, H_2-Kr, and H_2-Xe achieved excellent results using the "secular equation/perturbation theory" (SEPT) method of Ref. 59. However, the distinctly stronger potential anisotropy of the H_2-Kr system (compared to H_2-Ar) gives rise to substantially stronger interchannel coupling, and due to the accuracy of the new IR data,[34] the SEPT method is no longer adequate. The present work therefore uses the "iterative secular equation" (ISE) method of Ref. 60, which is essentially exact and has been used in a study of $He-C_2H_2$ and in the determination of accurate potential energy surfaces from spectroscopic data for He–CO.[10,11,61] However, the ISE method has never previously been used to simulate hyperfine transitions, and in the He–CO work,[10,11] the partial derivatives of level energies with respect to potential function parameters required by the least-squares procedure were determined by differences, a relatively tedious procedure. Two other aspects of the present work involve extending the ISE method to allow it both to generate analytic partial derivatives and to simulate the type of hyperfine transition observed by Waaijer and Reuss.[22]

In the following, the three-dimensional "exchange-Coulomb" (XC) potential energy model used herein, and the manner by which it can be modified or "morphed" by the fits to experimental data are described in Sec. II. Our enhanced version of the ISE method for calculating eigenvalues and eigenfunctions for vibration-rotation levels of atom-molecule complexes is described in Sec. III. The experimental data used and some aspects of the fitting procedure are then described in Sec. IV, and the resulting optimized XC potential energy surface for H_2-Kr is presented and compared with the best potential from the literature in Sec. V. Our conclusions are then summarized in Sec. VI, while the Appendix describes issues encountered in using the resulting recommended potential for practical calculations.

II. MODEL POTENTIAL USED FOR H_2-Kr

The earliest work in this field used either purely empirical model potential energy functions[1] or potential forms incorporating fixed, theoretically known anisotropic dispersion energy coefficients.[2–5,8–10] However, it would be virtually impossible to determine purely empirically a sufficiently large number of parameters to characterize fully the detailed shapes of the potential surfaces for systems with even moderately strongly anisotropic interactions. At the same time, in spite of remarkable advances in *ab initio* methods for describing weak interactions, for all but the simplest systems they are still unable to provide a fully satisfactory description of such interactions. On the other hand, *ab initio* or appropriately chosen model potential energy surfaces of even moderate quality should incorporate most qualitative features of the shape of the true surface. Thus, an increasingly common approach has been to start with a realistic theoretical potential energy function, and then to globally modify or morph it to optimize the agreement with experimental data, with the implicit assumption that the sound physics incorporated into the initial surface will make the refined potential quantitatively reliable in regions to which the data used in the analysis are not particularly sensitive. This is the approach used here.

A. Exchange-Coulomb potential for H_2-Kr

For interactions involving closed-shell species, a number of approaches have been suggested for constructing potential energy surfaces as a sum of (mainly) attractive and (mainly) repulsive components, each of which is obtained from a relatively inexpensive calculation.[7,11,38–58] These models can represent most important features of the interaction quite realistically, including effects due to the internal bond-length dependence of the component monomers. They typically model the main attractive part of the interaction energy using the best available long-range multipolar interaction energies, corrected for the neglect of charge overlap effects[62] through

the use of multiplicative damping and corrector functions. While other approaches use supermolecule self-consistent field (SCF) dimer interaction energies to represent the (mostly) repulsive part of the interaction energy, the exchange-Coulomb or XC model[7,11,45–47] used herein employs the Heitler–London interaction energy (the sum of the first-order Coulomb and exchange energies) for this purpose. Since it only requires the SCF wave functions for the interacting monomers, the XC model is, in principle, quite easy to apply.

The present work uses the Jacobi coordinates $\mathbf{r}=r\hat{\mathbf{r}}$, $\mathbf{R}=R\hat{\mathbf{R}}$, and θ, where $\mathbf{r}$ is a vector of length r joining the atoms in the diatom, $\mathbf{R}$ a vector of length R running from the midpoint of the diatom bond to the Kr atom, $\hat{\mathbf{r}}$ and $\hat{\mathbf{R}}$ are unit vectors, and $\theta\equiv\cos^{-1}(\hat{\mathbf{r}}\cdot\hat{\mathbf{R}})$. In practice, the diatom bond length r is replaced by the dimensionless stretching coordinate $\xi\equiv(r-r_0)/r_0$, where the fixed reference distance $r_0=1.448\,739a_0$ is the expectation value of r for H_2 in its ground rovibrational level.[63] As in our study of H_2-Ar,[7] the XC potential is then written as

$$V(R,\theta,\xi)=\mathfrak{F}E_{\mathrm{HL}}^{(1)}(R,\theta,\xi)+\Delta E_C(R,\theta,\xi)$$
$$=\mathfrak{F}E_{\mathrm{HL}}^{(1)}(R,\theta,\xi)-G_{12}(R,\theta)\times\sum_{n=6(2)}^{12}f_n(R,\theta)C_n(\theta,\xi)/R^n \quad (1)$$

with the long-range interaction coefficients being expanded as

$$C_n(\theta,\xi)=\sum_{\lambda=0(2)}^{n-4}C_n^{(\lambda)}(\xi)P_\lambda(\cos\theta), \quad (2)$$

in which $P_\lambda(\cos\theta)$ is the usual Legendre polynomial of order λ. Here, $E_{\mathrm{HL}}^{(1)}$ is the first-order Heitler–London interaction energy, and the main attractive part of the potential, ΔE_C, is an individually damped, overall-corrected, dispersion plus induction energy series representing the second- and higher-order Coulomb interaction energy. The individual damping functions f_n take account of non-negligible charge overlap effects on the individual R^{-n} multipolar contributions to the second-order Coulomb interaction energy and prevent these inverse-power terms from diverging at small R.[64,65] The amplifying "corrector" function G_{12} corrects for the omission of additional higher-order inverse-power terms from the potential model, as discussed below.[40,43,51] Finally, the quantity $\mathfrak{F}$ is an empirical scaling factor to be determined from a fit to experimental data, as discussed in Sec. II B.

Values of the Heitler–London interaction energy $E_{\mathrm{HL}}^{(1)}$ for H_2-Kr were calculated using a version of the CADPAC program[66] which incorporates the Hayes–Stone perturbation theory program.[67] The calculations are analogous to those reported earlier for a fixed H_2 bond length of $r=1.4a_0$,[68] and are based on high quality SCF wave functions for the isolated monomers.[69] Heitler–London energies were obtained at six equally spaced values of R ($3a_0\leqslant R\leqslant 8a_0$), four values of θ, and five H_2 bond lengths ($1.1a_0\leqslant r\leqslant 1.9a_0$).[70] These 120 computed energies were fitted to the form

TABLE I. Dimensionless parameters $a_{p,k}^{(\lambda)}$ defining our fit of Eq. (3) to our calculated Heitler–London energies for H_2-Kr. Other parameters involved in the fit are $K=(316.880\,673\,582\,54\times10^{-6})E_h$, $b_0=1.816\,53a_0^{-1}$, $b_1=0.3199a_0^{-1}$, $b_2=0.141a_0^{-1}$, and the expansion coefficients of Eq. (4): $R_m^{(0)}=7.049\,387\,8a_0$, $R_m^{(2)}=0.025\,668\,5a_0$, $R_m^{(4)}=-0.001\,307\,3a_0$, and $R_m^{(6)}=-0.000\,578\,9a_0$.

p	k	$\lambda=0$	$\lambda=2$	$\lambda=4$	$\lambda=6$
0	0	1.0	0.1814	0.0095	0.0014
1	0	0.0	−0.0742	−0.0137	0.0
2	0	0.0	0.296	−0.019	−0.021
3	0	0.0	0.0	−0.23	−0.08
0	1	1.3029	0.657	0.0459	0.005
1	1	3.145	0.432	−0.011	0.0
2	1	1.83	0.95	0.0	−0.12
3	1	0.0	0.0	−0.98	−0.5
0	2	0.632	0.832	0.107	0.01
1	2	4.0	2.01	0.09	0.0
2	2	7.9	2.4	0.0	0.2
3	2	5.4	0.0	−1.9	0.0
0	3	0.03	0.47	0.12	0.0
1	3	1.29	2.1	0.0	0.0
2	3	6.7	3.0	0.0	0.0
3	3	9.0	0.0	0.0	0.0

$$E_{\mathrm{HL}}^{(1)}(R,\theta,\xi)=Ke^{-(R-R_s)(b_0+b_1z+b_2z^2)}\times\sum_{k=0}^{3}\sum_{p=0}^{3}\sum_{\lambda=0(2)}^{6}a_{pk}^{(\lambda)}\xi^k z^p P_\lambda(\cos\theta), \quad (3)$$

in which $z\equiv(R-R_s)/(R+R_s)$, $a_{00}^{(0)}=1$, and $R_s=R_s(\theta)$ is a fixed reference distance function (see below). In this least-squares fit, the weight associated with each $E_{\mathrm{HL}}^{(1)}(R,\theta,\xi)$ datum was the inverse square of an uncertainty defined as 0.1% of its value. The individual $a_{pk}^{(\lambda)}$ coefficients defining this function have no particular physical significance, so the fact that a number of them are not statistically significant and are rounded to zero (see Table I) is of no concern.

Aside from the restriction to even Legendre angular functions, reflecting the homonuclear symmetry of H_2, and the fact that it dies off exponentially at large R, the algebraic form of Eq. (3) has no particular physical significance other than that it should give a good representation (relative to the chosen 0.1% relative uncertainties) of the 120 *ab initio* Heitler–London energies. However, we chose to define the (in principle, arbitrary) reference distance $R_s=R_s(\theta)$ as the position $R_m(\theta,\xi=0)$ of the (angle-dependent) radial potential minimum for the monomer stretching coordinate fixed at $\xi=0$. In practice, an initial representation of $E_{\mathrm{HL}}^{(1)}$ is obtained using some preliminary constant R_s value, and the resulting $E_{\mathrm{HL}}^{(1)}$ function is then combined with ΔE_C to yield an overall potential from which the actual $R_m(\theta,\xi=0)$ values may be determined. The latter are then fitted to the angular expansion

$$R_s(\theta)=R_m(\theta,\xi=0)=\sum_{\lambda=0(2)}^{6}R_m^{(\lambda)}P_\lambda(\cos\theta). \quad (4)$$

Repeating the fit to the $E_{\mathrm{HL}}^{(1)}$ data with R_s defined by iteratively refined versions of Eq. (4) yields rapid convergence to

TABLE II. Values of the $\{A_n\}$, $\{B_n\}$, and $\{D_n\}$ constants characterizing the damping functions $f_n(R,\theta)$ of Eq. (5), in atomic units (from Ref. 65).

	$n=6$	$n=8$	$n=10$	$n=12$
A_n	0.364 8	0.307 3	0.251 4	0.219 7
B_n	0.033 60	0.024 69	0.023 79	0.019 64
D_n	0.001 651	0.001 227	0.000 566 4	0.000 416 8

the desired self-consistent form. This approach yields a very precise representation of the *ab initio* $E_{\mathrm{HL}}^{(1)}$ values with discrepancies which are on average only 0.58 times the assigned (0.1%) uncertainties. The resulting constants K, b_i, $a_{pk}^{(\lambda)}$, and $R_m^{(\lambda)}$ defining this $E_{\mathrm{HL}}^{(1)}$ function are listed in Table I. Note that our particular definition of R_s affects our analytic representation of $E_{\mathrm{HL}}^{(1)}$, but does not significantly affect the shape of the resulting analytic function.

The multipolar representation used for ΔE_C [see Eq. (1)] is based on the best available values of the dispersion and induction coefficients $C_n(\theta,\xi)$,[71,72] and on the fixed damping and corrector functions

$$f_n(R,\theta) = [1 - e^{-A_n(SR)-B_n(SR)^2-D_n(SR)^3}]^n, \tag{5}$$

$$G_{12}(R,\theta) = 1 + 27.79e^{-0.6850(SR)-0.029\,98(SR)^2}, \tag{6}$$

in which S is a system-dependent scaling factor. Following a widely used approach,[38–40,43,51] these functions are defined by scaling the radial coordinate of the analogous functions determined for the nonbonded $H_2(^3\Sigma_u^+)$ interaction, which are known essentially exactly.[65,73,74] In particular, the constants A_n, B_n, and D_n are those determined for the $H_2(^3\Sigma_u^+)$ interaction (which corresponds to $S\equiv 1$);[65] they are listed in Table II. As in previous work,[7,11,38–50] the scaling factor S used to map the functions derived for $H_2(^3\Sigma_u^+)$ onto the range of the H_2–Kr potential is defined as $S=R_m^{H_2}/R_m(\theta,\xi=0)$, where $R_m^{H_2}=7.82a_0$ is the position of the $H_2(^3\Sigma_u^+)$ potential minimum. As outlined above, the values of $R_m(\theta,\xi=0)$, and hence of $S=S(\theta)$, are determined iteratively once the rest of the potential is specified. While $R_m(\theta)$ (and hence S) could also be expressed as a function of ξ, that would complicate the potential model, and since the effect of ξ on the potential energy surface in the region of interest is relatively modest, that ξ dependence is absorbed into other parts of the model. Note that in contrast to the situation for the representation of $E_{\mathrm{HL}}^{(1)}$, where the values of $R_m(\theta,\xi=0)$ affect the representation of the interaction but not its values, the fact that $R_s = R_m(\theta,\xi=0)$ characterizes the onset of the damping of the multipole expressions for the various dispersion energy terms means that it *does* affect the magnitude of the $\Delta E_C(R,\theta,\xi)$ contributions to the overall XC potential function.

Anisotropic dispersion and induction coefficients $C_n^{(\lambda)}(\xi)$ for H_2–Kr and other H_2–Rg interactions have been reported by Wormer, Hettema, and Thakkar,[71] the dispersion coefficients being calculated from dynamic multipole polarizabilities while the induction coefficients were generated from the multipole moments of H_2 and the static polarizabilities of the atoms. Vibrationally averaging these *ab initio* results for C_6 for the ground vibration-rotation state of H_2 yielded $\overline{C}_6^{(0)}$ and $\overline{C}_6^{(2)}$ values which were, respectively, some 2.58% and 5.04% higher than the accurate values determined by constrained dipole oscillator strength (DOSD) techniques.[72] The "theoretical" $C_6^{(0)}(\xi)$ and $C_6^{(2)}(\xi)$ values used here were therefore obtained by scaling the *ab initio* results of Ref. 71 to reproduce the DOSD values. The resulting set of long-range coefficients $C_n^{(\lambda)}(\xi)$ are listed in Table III, together with estimates of their uncertainties; for $n>6$ these values contain both dispersion and induction contributions. Note that in Eq. (1) we have assumed that the induction energy damping functions are the same as those for the corresponding dispersion terms. This cannot be justified theoretically, but little is known about the damping of induction energies for interactions involving molecules, and since the attractive part of the H_2–Kr interaction is dominated by the dispersion energy, error due to this approximate treatment of the induction damping has little effect.

In our analytic representation of $\Delta E_C(R,\theta,\xi)$, the theoretical long-range potential coefficients are expanded as

$$C_n^{(\lambda)}(\xi) = \sum_{k=0}^{k_{\max}^{(n,\lambda)}} C_n^{\lambda,k}\xi^k. \tag{7}$$

The fact that the H_2–Kr potential energy surface must collapse to the one-dimensional He–Kr potential curve as $\xi\rightarrow$

TABLE III. *Ab initio* values of composite dispersion and induction coefficients $C_n^{(\lambda)}(\xi)$ for H_2–Kr, in atomic units (Ref. 71). The values of $C_6^{(0)}$ and $C_6^{(2)}$ were scaled to reproduce the accurately known values obtained from dipole oscillator strength distribution (Ref. 72, see text), while the $r=0$ values (for He–Kr) are based on those of Ref. 76, but with $C_6^{(0)}$ scaled to take account of reliable DOSD results (Ref. 75). Values of $C_{12}^{(0)}$ were defined by Eq. (9) with uncertainties taken as ±55% for $r>0$ and ±100% for $r=0$.

r/a_0	ξ	$C_6^{(0)}$	$C_6^{(2)}$	$C_8^{(0)}$	$C_8^{(2)}$	$C_8^{(4)}$	$C_{10}^{(0)}$	$C_{10}^{(2)}$	$C_{10}^{(4)}$	$C_{10}^{(6)}$
0.0	−1.000	13.258	0.0	254.5	0.0	0.0	6 650.0	0.0	0.0	0.0
1.0	−0.310	28.947	1.6793	679.61	74.619	2.2671	19 345.0	2 350.2	68.618	12.068
1.2	−0.172	33.498	2.5322	809.43	124.53	5.119	23 625.0	4 129.6	202.31	23.895
1.4	−0.034	38.239	3.5537	951.61	194.49	9.6448	28 467.0	6 733.9	402.78	36.897
1.449	0.000	39.416	3.8288	988.1	215.06	11.029	29 731.0	7 515.8	464.78	40.453
1.65	0.139	44.264	5.0403	1143.5	315.18	18.136	35 215.0	11 396.0	803.44	58.548
2.0	0.381	52.462	7.3341	1430.3	557.59	36.379	45 792.0	21 259.0	1909.5	120.25
3.0	1.071	68.14	11.7626	2227.1	1804.4	120.21	80 049.0	80 925.0	13329.0	721.65
Uncertainty	$(r>0)$	±1%	±1%	±5%	±13%	±20%	±13%	±25%	±42%	±67%
Uncertainty	$(r=0)$	±5%		±15%			±30%			

-1 ($r\rightarrow 0$) means that $C_n^{(\lambda)}(\xi=-1)=0$ when $\lambda>0$.[4] This condition is used to define the value of the highest-order expansion coefficient for each combination of n and λ in terms of the others,

$$C_n^{\lambda,k_{\max}^{(n,\lambda)}}=(-1)^{k_{\max}^{(n,\lambda)}-1}\sum_{k=0}^{k_{\max}^{(n,\lambda)}-1}(-1)^k C_n^{\lambda,k}, \quad \text{for}\,\lambda>0. \tag{8}$$

For $\lambda=0$, however, this collapsed-diatom limit constraint was imposed by including the known values of the $C_n(He-Kr)$ coefficients[75,76] for $n=6$, 8, and 10 as $C_n^{(\lambda)}(\xi=-1)$ data in the fit to Eq. (7).

In our analogous study of H_2-Ar, the inverse-power expansion comprising the last term in Eq. (1) was truncated at the term varying as R^{-10}, and it was found that the potential could not adequately represent the experimental data unless that last term was scaled to be far stronger than was suggested by the theoretical $C_{10}^{(0)}(\xi)$ values.[7] This suggests that the fit to determine that potential was sensitive to the neglect of R^{-n} contributions for $n>10$. The present work therefore included an isotropic $n=12$ term in the inverse-power expansion of Eq. (1), but since no theoretical estimates are available, its values were approximated using a recursion relation suggested by Tang and Toennies:[55]

$$C_{12}^{(0)}(\xi)=C_6^{(0)}(\xi)[C_{10}^{(0)}(\xi)/C_g^{(0)}(\xi)]^3. \tag{9}$$

The corrector function G_{12} was determined[77] in the same manner as was the G_{10} function used in the earlier version of the XC potential energy model[38,40,43] in which the long-range dispersion energy expansion was truncated at the R^{-10} term. In particular, with the $f_n(R,\theta)$ functions defined by Eq. (5), the parameters defining G_{12} were determined by fitting the accurately known values of $\Delta E_C(R)$ for the $H_2(^3\Sigma_u^+)$ interaction to the expression $-G_{12}(R)\Sigma_{n=6(2)}^{12}f_n(R)C_n/R^n$.

Our preliminary or *a priori* version of the XC potential for H_2-Kr, identified herein as the "XC(0)" surface, is given by Eqs. (1)–(9) with $\mathfrak{F}=1$, $E_{\mathrm{HL}}^{(1)}$ defined by the fit of the calculated energies to Eq. (3) yielding the coefficients listed in Table I, and the expansion coefficients $C_n^{\lambda,k}$ of Eq. (7) determined purely from fits to the theoretical values listed in Table III. While realistic, this three-dimensional potential is not expected to be quantitatively accurate. The rest of this work is concerned with using a fit to experimental data to determine the optimized "XC(fit)" potential for this system.

B. Fitting a XC model potential to experimental data

Part of the success of the XC potential function model in yielding reliable (rare gas)–(rare gas) and (rare gas)–molecule potentials[7,11,41–47] has been due to recognition of the fact that since theoretical inverse-power long-range potential coefficients are usually not exact, fits to experimental data should allow those coefficients to vary within their estimated uncertainties.[78,79] In contrast, in most previous modeling of multidimensional van der Waals potential energy surfaces, the long-range potential energy coefficients were held fixed at the best estimates yielded by theory. That approach overlooks the uncertainties in those calculated values, uncertainties which tend to increase rapidly with n and λ, and it introduces an unnecessary and inappropriate degree of rigidity into a potential model.

Following Refs. 11 and 7, the present work treats the theoretical $C_n^{(\lambda)}(\xi)$ values of Table III as "*ab initio* data" and simply includes them with the spectroscopic line positions in the least-squares fit analysis. This in turn makes the $C_n^{\lambda,k}$ coefficients of Eq. (7) free parameters in the fit. While this might appear to introduce an excessive number of empirical parameters, in practice their values are mainly determined by the *ab initio* $C_n^{(\lambda)}(\xi)$ "data," and for the most part are only modestly affected by the spectroscopic data. Moreover, because those data are not particularly sensitive to their ξ dependence, the anisotropic dispersion coefficients (those for $\lambda>0$) were were fitted as groups represented by the expressions

$$C_n^{(\lambda)}(\xi)=Q_n^{(\lambda)}\sum_{k=0}^{k_{\max}^{(n,\lambda)}}C_{n,\mathrm{th}}^{\lambda,k}\xi^k, \tag{10}$$

in which the coefficients $C_{n,\mathrm{th}}^{\lambda,k}$ (in which th denotes "theory") are fixed values determined purely from independent fits to the theoretical $C_n^{(\lambda)}(\xi)$ values of Table III to Eq. (7), and only the group scaling parameters $Q_n^{(\lambda)}$ were allowed to vary in the global analysis.

Treating the $C_n^{\lambda,k}$ [or $Q_n(\lambda)$] parameters as variables certainly provides a degree of flexibility in XC potential energy surface. However, the main means of modifying the *a priori* XC(0) surface to optimize the agreement with experimental data is through the factor $\mathfrak{F}$ which scales the mainly repulsive Heitler–London part of the interaction energy. It is expected to be a weak function of R, θ, and ξ.[7,11,45–47] However, in the present work it proved adequate to represent it as a function of θ and ξ only:

$$\mathfrak{F}=\mathfrak{F}(\theta,\xi)=\sum_{\lambda=0(2)}^{\lambda_{\max}^{(\mathfrak{F})}}\sum_{k=0}^{k_{\max}^{(\mathfrak{F})}}F_{\lambda,k}\xi^k P_\lambda(\cos\theta). \tag{11}$$

More sophisticated parametrizations of $\mathfrak{F}$ were also examined, but the resulting marginal improvement in the quality of fit to the experimental data did not justify the increased complexity.

In summary, the free parameters varied in the fit to the XC model potential for H_2-Kr are the $F_{\lambda,k}$ expansion parameters of Eq. (11), plus the individual $C_n^{\lambda,k}$ expansion coefficients for some combinations of λ and n, and the group scaling parameters $Q_n^{(\lambda)}$ for others. The *a priori* initial trial XC(0) surface, which has *no* empirical parameters, is obtained by setting $F_{0,0}=1$ and all other $F_{\lambda,k}=0$, fixing all $Q_n^{(\lambda)}=1$ and setting all $C_n^{\lambda,k}$ coefficients at the values $C_{n,\mathrm{th}}^{\lambda,k}$ obtained from fits to the sets of *ab initio* $C_n^{(\lambda)}(\xi)$ values.

III. COMPUTATIONAL METHODS

The previous generation[21,23] of infrared data for H_2-Kr (those used to determine the potential function of Ref. 6) had line position uncertainties of $\lesssim 0.02\ \mathrm{cm}^{-1}$, and the SEPT procedure of Ref. 59 yielded a more than adequate level of accuracy for the requisite calculations. However, the new

data of Ref. 34 are substantially improved, with typical estimated uncertainties of $\pm 0.004\ \mathrm{cm}^{-1}$ and the SEPT method proved to be no longer adequate. In particular, for a realistic trial H_2-Kr potential, comparisons with results generated using Hutson's (essentially exact) BOUND program[80] showed that for truly bound states the SEPT method could yield eigenvalue predictions with errors of up to $0.008\ \mathrm{cm}^{-1}$, approximately twice the uncertainty of the new line positions.[34] On the other hand, while BOUND gives quite reliable eigenvalues, it does not take account of the shifting and broadening of metastable levels and cannot readily yield the wave functions required for direct calculation of the partial derivatives with respect to potential parameters needed for a least-squares fitting procedure. Thus, a better method was required.

The method for calculating the transition frequencies (and predissociation linewidths) used herein is the fully recontracted version of the ISE method of Slee and Le Roy.[60] As is BOUND, this method is also (in principle) exact for truly bound states, and ISE eigenvalues calculated for H_2-Kr agreed with those generated from BOUND to within $10^{-5}\ \mathrm{cm}^{-1}$ for all truly bound states of H_2-Kr. The ISE method is also very efficient, with a computational effort which grows relatively slowly with the number of coupled channels, and since it gives wave functions naturally, it may readily be adapted to calculate spectroscopic intensities or to apply a Hellman–Feynman theorem procedure to calculate the partial derivatives required by the fitting procedure. Moreover, its structure very naturally incorporates a perturbative treatment of the coupling to open and to distant closed channels.

A. Calculating derivatives with respect to potential energy function parameters within the ISE method

In each cycle of a nonlinear least-squares fitting procedure, values of the partial derivatives of the calculated value of each observable with respect to each parameter of the model are required. In our previous applications of the ISE and SEPT methods,[6,7,10,11] the partial derivatives of the observed transition energies with respect to the potential energy function parameters were calculated numerically from symmetric first differences. However, the computational cost of that approach is high, since for each cycle of a fit to a potential energy model with N_p fitting parameters the whole simulation must be performed some $2N_p+1$ times. In the present work we therefore implemented the Hellman–Feynman theorem for calculating the partial derivatives of the eigenvalues directly.

For an atom-diatom van der Waals molecule, the Hamiltonian governing the nuclear motion may be written as

$$\tilde{H}_0(\mathbf{R},\mathbf{r}) = -\frac{\hbar^2}{2\mu_{\mathrm{d}}}\nabla^2 - \frac{\hbar^2}{2\mu_{\mathrm{da}}}\nabla_R^2 + V(R,\theta,\xi), \tag{12}$$

in which μ_d is the normal reduced mass of the component diatom and μ_{da} the analogous reduced mass for the diatom-atom pair. The Hellman–Feynman theorem tells us that for a particular eigenvalue E_α of this Hamiltonian, the partial derivative with respect to p_i, one of the parameters defining the potential energy function $V(R,\theta,\xi)$ is

$$\frac{\partial E_\alpha}{\partial p_i} = \left\langle \Psi_\alpha \left| \frac{\partial V(R,\theta,\xi)}{\partial p_i} \right| \Psi_\alpha \right\rangle, \tag{13}$$

where $\Psi_\alpha = \Psi_\alpha(\mathbf{r},\mathbf{R})$ is the eigenfunction of $\tilde{H}_0$ corresponding to eigenvalue E_α. In a coupled-channel method the eigenfunctions of $\tilde{H}_0$ may be expanded as

$$\Psi_\alpha(\mathbf{r},\mathbf{R}) = \sum_a \chi_a^\alpha(R)\Phi_a^{JM_J}(\mathbf{r},\hat{\mathbf{R}}), \tag{14}$$

where α is the state label and $\Phi_a^{JM_J}(\mathbf{r},\hat{\mathbf{R}})$ is the basis function characterizing a particular channel a. In the space-fixed coordinate system used here, $\alpha=\{v,j,n_v,l,J,M_J\}$ and the channel index $a=\{v,j,l\}$, where v and j are the vibrational and rotational quantum numbers for the H_2 diatom, n_v and l are the quantum labels for the stretching vibration and rotation of the van der Waals bond axis R, and J and M_J are the total rotational angular momentum quantum number and its space-fixed projection. In addition, the space-inversion parity p and the parity for permutation of two hydrogen atoms s are conserved quantities, but to simplify the notation they are usually not shown. Of these indices, only $\{J,M_J,p,s\}$ are truly good quantum numbers of $\tilde{H}_0$, although the monomer vibrational index v is usually a near-exact quantum number and n_v is an unambiguous state label. For complexes formed from diatomic hydrogen, a single value of j always dominates the wave function for any discrete state and l is an approximate quantum number which provides a useful zeroth order ordering of the various states. For other species, however, j mainly serves as convenient "uncoupled limit" state-ordering label and l is completely mixed.

In the ISE method, the overall rotation and diatom vibration basis functions characterizing the various coupled channels have the form

$$\Phi_a^{JM_J}(\mathbf{r},\hat{\mathbf{R}}) = \varphi_{vj}(r)\mathcal{Y}_{jl}^{JM_J}(\hat{\mathbf{r}},\hat{\mathbf{R}}), \tag{15}$$

in which $\varphi_{vj}(r)$ is a radial wave function for a free diatomic hydrogen molecule and

$$\mathcal{Y}_{jl}^{JM_J}(\hat{\mathbf{r}},\hat{\mathbf{R}}) = \sum_{m_j,m_l} C(j,l,J;m_j,m_l,M_J)Y_{j,m_j}(\hat{\mathbf{r}})Y_{l,m_l}(\hat{\mathbf{R}}) \tag{16}$$

are the usual total orbital angular momentum eigenfunctions for an atom-linear molecule system, defined as linear combinations of products of the spherical harmonic eigenfunctions $Y_{j,m_j}(\hat{\mathbf{r}})$ and $Y_{l,m_l}(\hat{\mathbf{R}})$ associated with the free rotation of the diatom and of the molecular axis $\hat{\mathbf{R}}$, respectively, and $C(j,l,J;m_j,m_l,M_J)$ are Clebsch–Gordon coefficients. Since the interaction potential for the H_2 diatom is accurately known,[63] accurate diatom eigenfunctions $\varphi_{vj}(r)$ may be readily generated using standard methods.[81]

A convenient feature of the XC potential form is the fact that it is a linear function both of the fitting parameters $F_{\lambda,k}$ and $C_n^{\lambda,k}$ coefficients and of the powers of the diatom stretching coordinate ξ. This means that it may be written in the form

$$V(R,\theta,\xi) = \sum_{k=0}^{k_{\max}} \xi^k V_k(R,\theta)$$
$$= \sum_{k=0}^{k_{\max}} \xi^k \sum_{\lambda=0(2)}^{\lambda_{\max}} V_{\lambda,k}(R) P_\lambda(\cos\theta)$$
$$= \sum_{i\geqslant 1} p_i \sum_{k=0}^{k_{\max}} \xi^k W_{k,i}(R,\theta)$$
$$= \sum_{i\geqslant 1} p_i \sum_{k=0}^{k_{\max}} \xi^k \sum_{\lambda=0(2)}^{\lambda_{\max}} W_{k,i}^{(\lambda)}(R) P_\lambda(\cos\theta), \quad (17)$$

in which $\{p_i\}$ are the adjustable parameters $\{F_{\lambda,k}\}$, $\{Q_n^{(\lambda)}\}$, and $\{C_n^{\lambda,k}\}$ of Eqs. (11), (10), and (7), respectively, and the functions $W_{k,i}(R,\theta) \equiv \partial V_k(R,\theta)/\partial p_i$ and $W_{k,i}^{(\lambda)}(R)$ are properties of the XC(0) surface and do not change from one cycle of the fit to the next. Since the $E_{\mathrm{HL}}^{(1)}$ component of the XC potential form is not a simple linear function of the Legendre functions $P_\lambda(\cos\theta)$, the $W_{k,i}^{(\lambda)}(R)$ [and $V_{\lambda,k}(R)$] functions are determined numerically by orthogonal projection

$$W_{k,i}^{(\lambda)}(R) = \langle P_\lambda(\cos\theta) | W_{k,i}(R,\theta)\rangle. \quad (18)$$

However, this calculation need only be done once, and the resulting one-dimensional radial (in R) arrays stored for repeated use throughout the fit. The computational effort saved by this step is quite significant, a point favoring potential functions of this form. In the present work it was found that these radial functions need only be generated for $\lambda \leqslant 6$; extending the angular series to $\lambda = 12$ affected the H_2-Kr eigenvalues by less than 0.000 01 cm^{-1}.

The partial derivatives required by the least-squares fitting procedure may be written as

$$\langle \Psi_\alpha | \partial V/\partial p_i | \Psi_\alpha\rangle = \int dR \sum_{a,a'} \chi_a^\alpha(R)\chi_{a'}^\alpha(R) \times (\Phi_a^{J,M_J} | \partial V(R,\theta,\xi)/\partial p_i | \Phi_{a'}^{J,M_J}), \quad (19)$$

in which the notation $(\Phi_a^{J,M_J}|\ldots|\Phi_{a'}^{J,M_J})$ implies integration over all coordinates except R.[82] Using Eqs. (15) and (17),

$$(\Phi_a^{J,M_J} | \partial V(R,\theta,\xi)/\partial p_i | \Phi_{a'}^{J,M_J})$$
$$= \sum_{k=0}^{k_{\max}} \langle \varphi_{vj} | \xi^k | \varphi_{v'j'}\rangle (\mathcal{Y}_{jl}^{JM_J} | W_{k,i}(R,\theta) | \mathcal{Y}_{j'l'}^{JM_J})$$
$$= \sum_{k=0}^{k_{\max}} \langle \varphi_{vj} | \xi^k | \varphi_{v'j'}\rangle \sum_{\lambda=0}^{\lambda_{\max}} W_{k,i}^{(\lambda)}(R) f_\lambda(j,l;j',l';J), \quad (20)$$

in which $f_\lambda(j,l;j',l';J) = \langle \mathcal{Y}_{jl}^{JM_J} | P_\lambda(\cos\theta) | \mathcal{Y}_{j'l'}^{JM_J}\rangle$ are Percival–Seaton coefficients (which do not depend on M_J).[83,84] As mentioned above, at a chosen grid of points $\{R_i\}$ the various radial functions $W_{k,i}^{(\lambda)}(R_i)$ may be calculated once and stored for use in all subsequent eigenvalue derivative calculations and all subsequent fit iterations. In the present case, the radial grid used typically has ca. 3000 points and only 70–90 different radial functions are required, so the storage requirements are quite modest. Note too that the derivatives of the $C_{n'}^{(\lambda')}(\xi)$ data required by the fit are readily generated, since their derivatives with respect to the $F_{\lambda,k}$ are identically zero, and when $C_{n'}^{(\lambda')}(\xi)$ is represented by Eq. (7) we have

$$\partial C_{n'}^{(\lambda')}(\xi)/\partial C_n^{\lambda,k} = \delta_{nn'}\delta_{\lambda\lambda'}\xi^k, \quad (21)$$

while when Eq. (10) is used for $C_{n'}^{(\lambda')}(\xi)$ we have

$$\partial C_{n'}^{(\lambda')}(\xi)/\partial Q_n^{(\lambda)} = \delta_{nn'}\delta_{\lambda\lambda'} \sum_{k=0}^{k_{\max}^{(n,\lambda)}} C_{n,\mathrm{th}}^{\lambda,k}\xi^k. \quad (22)$$

B. Hellman–Feynman derivatives for a hyperfine transition

On taking account of nuclear spin **I**, the total Hamiltonian for our H_2-Rg systems may be written as the sum of the nuclear motion Hamiltonian plus a hyperfine Hamiltonian operator,

$$\tilde{H}_{\mathrm{tot}} = \tilde{H}_0(\mathbf{R},\mathbf{r}) + \tilde{H}^{\mathrm{HF}} \quad (23)$$

and the total angular momentum becomes

$$\mathbf{F} = \mathbf{I} + \mathbf{J} = \mathbf{I} + \mathbf{j} + \mathbf{l}, \quad (24)$$

in which F and M_F replace J and M_J as the good quantum numbers, the state label becomes $m=\{v,j,n_v,l,J,I,F,M_F\}$ and the angular basis expands to include the nuclear spin eigenfunctions $Y_{I,M_I}(\hat{\mathbf{I}})$. In this case the total angular momentum wave functions become

$$\mathcal{Z}_{jlJI}^{FM_F} = \sum_{M_J,m_I} C(J,I,F;M_J,M_I,M_F)\mathcal{Y}_{jl}^{JM_J}(\hat{\mathbf{r}},\hat{\mathbf{R}})Y_{I,m_I}(\hat{\mathbf{I}}) \quad (25)$$

and the total basis functions characterizing the different channels are the product functions $\varphi_{vj}(r)\ \mathcal{Z}_{jlJI}^{FM_F}$.

The present discussion of hyperfine splittings in $H_2(v=0,j=1)-Kr$ assumes that I is a good quantum number with the *ortho*-H_2 value of $I=1$. As a result, when the nuclear spin/nuclear spin (SS) and nuclear spin/rotation (SR) interaction terms for the H_2 molecule are included in the Hamiltonian, $\tilde{H}^{\mathrm{HF}} = \tilde{H}^{\mathrm{SS}} + \tilde{H}^{\mathrm{SR}}$, each J level of a complex formed from *ortho*-H_2 is split to three levels, corresponding to $F=J-1$, J, and $J+1$. Since the matrix elements of the hyperfine Hamiltonian terms are typically 10^5 times smaller than the spacings between adjacent nuclear motion levels for these species, the hyperfine level shifts may be evaluated using first order perturbation theory, as the expectation value of $\tilde{H}^{\mathrm{HF}}$ over the total wave function.[59] Because the off-diagonal coupling between different J values is very weak, those terms are neglected and J treated as a good quantum number.[59,85] Moreover, the matrix elements of $\tilde{H}^{\mathrm{HF}}$ with the basis functions of Eq. (25) happen to be diagonal in l and the Hamiltonian matrix is block diagonal in $\{F,M_F,I,J,p,s\}$.

Because of the weakness of the $\tilde{H}^{\mathrm{HF}}$ interaction, it is also reasonable to neglect it in the ISE eigenvalue calculations which determine the total wave function for level m

TABLE IV. Experimental diatom vibration-rotation energies $E_d(v,j)$ (in cm^{-1}) which define the asymptotes of the radial channel potentials involved in the calculations.

	v	$j=0$	$j=1$	$j=2$	$j=3$	$j=4$	$j=5$
H_2	0	0.0	118.486 75	354.373 50	705.518 86	1 168.798 23	1 740.189 10
	1	4 161.168 7	4 273.741 44	4 497.839 10	4 831.392 15	5 271.380 40	5 813.922 86
	2	8 087.005 0	8 193.798 15	8 406.365 0	8 722.705 65	9 139.902 5	9 654.201 1
	3	11 782.360 0	11 888.510 0	12 084.701 15	12 384.084 27	12 778.818 95	13 265.276 77
D_2	0	0.0	59.780 42	179.064 10	357.314 42	593.716 80	887.214 42
	1	2 993.610 0	3 051.284 72	3 166.359 6	3 338.302 62	3 566.324 7	3 849.405 72
	3	5 868.149	5 923.746	6 034.678	6 200.426	6 420.220	6 693.056
	3	8 625.71	8 679.24	8 786.11	8 945.73	9 157.42	9 420.29

$$\Upsilon_m = \sum_{a,n_v} c^{(m)}_{n_v,a} \phi^a_{n_v}(R) \varphi_{v_j}(r) \mathcal{Z}^{FM_F}_{jlJI}, \tag{26}$$

in which $\phi^a_{n_v}(R)$ is a radial basis function ($n_v=0,1,\ldots$) for channel a, as determined by the ISE procedure.[86] The sensitivity of a hyperfine transition energy to the intermolecular potential therefore arises from the fact that it is sensitive to the precise mix of the different channel basis functions in this overall wave function:

$$\frac{\partial E^{\mathrm{HF}}}{\partial p_i} = 2\left\langle \Upsilon_m \middle| \tilde{H}^{\mathrm{HF}} \middle| \frac{\partial \Upsilon_m}{\partial p_i} \right\rangle. \tag{27}$$

For an infinitesimal change δ_{p_i} in one of the potential parameters, the effect on the total wave function of the resulting change in the Hamiltonian $\delta\tilde{H}_{\mathrm{tot}}$ may be calculated by perturbation theory, and the associated first-order wave function yields

$$\frac{\partial \Upsilon_m}{\partial p_i} = \sum_{m' \neq m} \frac{\langle \Upsilon_m | \partial V/\partial p_i | \Upsilon_{m'} \rangle}{E_m - E_{m'}} \Upsilon_{m'}, \tag{28}$$

in which the numerator involves the same potential derivative matrix elements seen in Eq. (19). Because the Hamiltonian is block diagonal in $\{F,M_F,J,I,p,s\}$ and matrix elements of $\tilde{H}^{\mathrm{HF}}$ are diagonal in l, the m' summation only runs over channel basis functions with labels $\{v',j',n'_v\} \neq \{v,j,n_v\}$:

$$\langle \Upsilon_m | \tilde{H}^{\mathrm{HF}} | \Upsilon_{m''} \rangle = \sum_{v,j,n_v,v',j',n'_v,l} c^{(m)}_{a,n_v} c^{(m'')}_{a',n'_v} \times (\mathcal{Z}^{FM_F}_{jlJI} \varphi_{vj} | \tilde{H}^{\mathrm{HF}} | \mathcal{Z}^{FM_F}_{j'lJI} \varphi_{v'j'}) \langle \phi^a_{n_v} | \phi^{a'}_{n'_v} \rangle, \tag{29}$$

in which $a=\{v,j,l\}$ and $a'=\{v',j',l\}$, and the hyperfine matrix elements $(\mathcal{Z}^{FM_F}_{j'lJI} \varphi_{vj} | \tilde{H}^{\mathrm{HF}} | \mathcal{Z}^{FM_F}_{j'lJI} \varphi_{v'j'})$ are generated from the H_2 spin coupling constants, as described in Refs. 85 and 59. Note that an approximation implicit in our use of the Feynman–Hellman theorem for hyperfine transitions is that the wave function is actually a normalized eigenfunction of the Hamiltonian $\tilde{H}_0$ and not of H^{HF} or $\tilde{H}_{\mathrm{tot}}$. However, in view of the small magnitude of the hyperfine splittings, this should introduce negligible error.

C. General considerations and treatment of metastable levels

All assigned observed IR transitions of H_2–Kr and D_2–Kr are associated with ground $n_v=0$ van der Waals bond stretching levels, and the anisotropic coupling is fairly weak. The zeroth order secular equation basis used in our ISE calculations therefore consists of all radial eigenstates supported by the effective radial "distortion" potential[59] associated with the dominant channel. In practice, this means that two zeroth order basis functions were used for levels correlating with small values of l, and one for large-l states. All of the corrections iteratively generated by the ISE procedure were combined (recontracted) into a single effective radial correction function for each channel,[60] which means in practice that ISE iterations past the first one used a total of three basis functions for small l levels and two for large-l ones.

In the calculations reported herein, values of the atomic masses and physical constants were taken from Ref. 87. As no Kr isotope splittings were observed in the infrared spectra, the spectroscopic data simulations were performed using the mass of the most common isotope, ^{84}Kr (57% natural abundance). Note, however, that use of the abundance-averaged atomic mass yields a reduced mass differing by only 0.003%, a change which would have a negligible effect on the calculated results. The H_2 and D_2 monomer level energies $E_d(v,j)$ which define the asymptotes of the various radial channel potentials used in the calculations are listed in Table IV; it is important to specify these values, since it is the differences between the observed transition energies and these reference spacings which allows information regarding the ξ dependence of the intermolecular potentials to be determined empirically.

While the (essentially exact) ISE method for truly bound states is explained fully in Ref. 60, the associated treatment of metastable states deserves further comment. An exact treatment of metastable states would generally require the use of scattering theory methods, which are not readily compatible with an iterative fitting analysis of discrete spectroscopic data. We therefore followed the approach of Refs. 60 and 10 in using approximate methods to calculate the effects of open channels on the energies and widths of such levels.

As discussed in Ref. 60, two types of metastable levels must be considered. The first are "Feschbach predissociation" levels: these are levels of the zeroth-order effective

one-dimensional distortion potential[59] associated with the dominant channel, which lie above the dissociation asymptote for one or more of the channels to which it is coupled. For example, a "bound" (low l) state of $H_2(v=1,j=2)-Kr$ lies above the asymptotes both for rotational predissociation to yield $H_2(v=1,j=0)$ and for vibrational predissociation to yield $H_2(v=0,j\leqslant 8)$. The level shift and broadening due to this type of coupling is calculated using the Feschbach formalism used in the SEPT procedure of Ref. 59. Such calculations are perturbative and can, in principle, be performed without including any basis functions for the open channels in the ISE basis. However, to improve our accuracy, basis functions associated with any bound levels of the distortion potential for such open channels were always included in our ISE basis so that only coupling to the continuum component of the open channel had to be estimated by perturbation theory. The natural incorporation of this perturbative treatment of level shifts and broadening due to open (or distant closed) channels into the normal computational procedure is one of the great advantages of the ISE method.

As discussed in Ref. 60, errors in level energies due to this perturbative treatment are generally expected to be only a small fraction of the level widths, although the errors in the analogously calculated widths could be somewhat larger, particularly for very long-lived states. To allow for this additional source of uncertainty, the total uncertainty used to weight experimental transition frequency "i" involving one of these Feschbach-metastable levels was

$$u_{\mathrm{tot},i} = \sqrt{(u_{\mathrm{exp},i})^2 + (0.2\Gamma_m)^2}, \tag{30}$$

in which $u_{\mathrm{exp},i}$ is the estimated experimental line position uncertainty and Γ_m the total calculated width for the predissociating upper or lower level m.

The second type of metastable behavior is the "tunneling predissociation" of levels which lie above the dissociation limit associated with the diatom vibration-rotation energy $E_d(v,j)$ correlated with that particular state, but are bound behind a (mainly) centrifugal potential energy barrier associated with the effective diagonal potential[86] for the dominant contributing channel. This type of predissociation affects the highest observed l levels of complexes formed from H_2 or D_2 in any given internal (v,j) state. Following Ref. 60, the effective radial channel basis functions used to represent such "quasibound" levels were determined using the Airy function boundary condition,[88] with the tunneling predissociation width being calculated semiclassically.[88,89] Single-channel tunneling predissociation widths obtained in this way are accurate to within a few percent of their magnitude, and the associated level energies are also accurate to within a few percent of those widths. This is as good as the accuracy with which the widths and positions of predissociation broadened lines may be measured experimentally, and hence is satisfactory for present purposes. Note that these tunneling level widths would be combined with any Feschbach predissociation contributions to yield the total level width Γ_m of Eq. (30).

One minor extension of this second procedure introduced here concerns the large-R cutoff of radial basis functions $\phi^a_{n_v}(R)$ associated with tunneling-predissociation levels. In the conventional treatment,[81,88] the outer boundary condition imposed on the quasibound (tunneling) level wave function requires it to match an inwardly increasing Airy function at the third turning point $R_3=R_3(E)$ on the outer wall of the effective potential barrier, and on convergence the resulting radial eigenfunction is normalized on the interval $[0,R_3]$ and set to zero for $R>R_3$. However, values of that function would abruptly drop to zero at the first radial mesh point past R_3. While it has no effect on the calculated single-channel level energy or width, this discontinuity is inappropriate for a realistic radial channel function and tends to cause instabilities when such functions are used later in the ISE procedure. To correct for this, after the Airy function boundary condition has been applied in the usual way, the resulting eigenfunction is propagated outward to the first node past R_3 and truncated there.

Note that the perturbative Feschbach formalism treatment of the effect of open channels on level energies and widths also applies to quasibound (tunneling-predissociation) levels which are coupled to channels sharing the same dissociation limit (i.e., have the same v and j) but have different l values. Thus, as far as coupling to open channels is concerned, bound and quasibound levels are treated using the approximate SEPT procedure.[59] While this introduces some additional error, only a small fraction of the assigned transitions involve quasibound levels, and most of them have moderately large widths which leads to them being substantially deweighted by Eq. (30). Thus, this small additional possible source of computational error should not affect our analysis significantly.

IV. THE ANALYSIS

A. Data used in the analysis

The experimental data set used in the present work consists of McKellar's new IR data for H_2-Kr and D_2-Kr and the one hyperfine transition for H_2-Kr reported by Waaijer and Reuss.[22,34] There are two key differences between the new IR data and those used in the most recent previous analysis.[6] The first is the substantially improved precision and larger number of assigned transitions; the line position uncertainties associated with most of the new data are 0.004 cm^{-1}, which is almost an order of magnitude better than the 0.02–0.03 cm^{-1} of the measurements used in Ref. 6. This improved resolution allowed many of the lines in the congested P- and R-branch regions of the H_2-Kr $Q_1(1)$ and $S_1(0)$ spectra to be resolved, and comparisons with simulated spectra allowed many (though not all) of those lines to be assigned uniquely so they could be used in the analysis.

The second important feature of the new IR results is the first-time observation of transitions associated both with the pure rotation $S_0(0)$ transitions of H_2-Kr and with the $Q_1(0)$ vibration-rotation transitions of D_2.[34] When combined with the existing [$S_1(0)$, $Q_1(1)$ and $S_1(1)$] vibration-rotation data types, the former make the analysis much more directly sensitive to the ξ dependence of the potential anisotropy. Similarly, the new $Q_1(0)$ $(\Delta v=1, j'=j''=0)$ data for D_2-Kr substantially improves the ability of the data set to delineate the ξ dependence of the isotropic part of the potential energy

surface. Unfortunately, in contrast with the most recent IR study of H_2-Ar,[24] the new H_2-Kr and D_2-Kr experiments were unable to resolve transitions involving either the excited $n_v=1$ van der Waals bond stretching levels or vibrational overtone $\Delta v=2$ transitions of hydrogen. However, this new data set is certainly much more sensitive to the details of the potential anisotropy in the attractive well region than were the earlier measurements.

In summary, the present analysis simultaneously fits to 143 mid- and far-IR transition frequencies for H_2-Kr and 76 for D_2-Kr.[34] This is more than three times as many uniquely assigned lines as were used in the fit which determined the best previous potential for this system.[6] The one hyperfine transition of $H_2(0,1)-Kr$ reported by Waaijer and Reuss,[22] which provides a very sharp measure of the radial average of the potential anisotropy for a complex formed from ground state *ortho*-H_2, was also included in the experimental data set. Finally, the data being fitted also included the 74 [including $C_{12}^{(0)}$ values generated from Eq. (9)] nonzero theoretical $C_n^{\lambda}(\xi)$ values listed in Table III, each weighted by the inverse square of the associated uncertainty.

B. Aspects of the fitting procedure

The present work uses an automatic nonlinear least-squares fitting procedure to simultaneously optimize the agreement with the three different types of data: (i) the $N_{\rm ir}=219$ infrared transition frequencies (ir), (ii) the $N_{\rm hf}=1$ hyperfine transition frequency (hf), and (iii) the $N_{\rm th}=74$ nonzero theoretical values of $C_n^{(\lambda)}(\xi)$ (th). The ability of the model to reproduce the N_γ known values of property γ ($\gamma=$ir, hf, or th) is characterized by the dimensionless root mean square deviation for that property,

$$\overline{dd}_\gamma=\left\{\frac{1}{N_\gamma}\sum_{i=1}^{N_\gamma}[Y_{\gamma,i}^{\rm obs}-Y_{\gamma,i}^{\rm calc}]^2/(u_{\gamma,i})^2\right\}^{1/2}, \tag{31}$$

in which $Y_{\gamma,i}^{\rm obs}$ is the known or observed value of the property Y_γ, $Y_{\gamma,i}^{\rm calc}$ the calculated value, and $u_{\gamma,i}$ is the associated uncertainty. As mentioned above, for the IR data involving metastable levels these uncertainties are generated using Eq. (30). A given value of $\overline{dd}_\gamma$ indicates that, on average, the calculated values disagree with experiment by $\overline{dd}_\gamma$ times the uncertainty in the data. The global dimensionless root mean square deviation minimized by the fit is then defined as

$$\overline{dd}_{\rm tot}=\{(N_{\rm ir}\overline{dd}_{\rm ir}^2+N_{\rm hf}\overline{dd}_{\rm hf}^2+N_{\rm th}\overline{dd}_{\rm th}^2)/N_{\rm tot}\}^{1/2}, \tag{32}$$

where $N_{\rm tot}=(N_{\rm ir}+N_{\rm hf}+N_{\rm th})$. Similarly, the value of $\overline{dd}_{\rm exp}=\{(N_{\rm ir}\overline{dd}_{\rm ir}^2+N_{\rm hf}\overline{dd}_{\rm hf}^2)/(N_{\rm ir}+N_{\rm hf})\}^{1/2}$ is a measure of the ability of the parametrized potential model to reproduce the experimental spectroscopic data, while the value of $\overline{dd}_{\rm th}$ indicates the quality of fit to the $C_n^{(\lambda)}(\xi)$ values of Table III.

To avoid problems due to incorrect spectroscopic assignments, the initial stage of the analysis only used the completely unambiguously assigned $Q_1(0)$ IR bands and N and T branches of the $Q_1(1)$, $S_0(0)$, and $S_1(0)$ IR bands. However, as the analysis proceeded and the value of $\overline{dd}_{\rm exp}$ approached unity, assignments for a large number of additional lines became unambiguous, and they were added to the data set. The few observed peaks in the IR spectra which had more than one possible assignment were omitted from the fit.

Following Ref. 90 the convergence of our nonlinear fits was determined by requiring that the changes in all parameters be less than the associated "parameter sensitivities," and the numbers of significant digits required to fully represent each of the final fitted parameters was minimized using the sequential rounding and refitting procedure described therein.

V. RESULTS

A. Optimized XC potential energy surface for H_2-Kr

A simulation of the data using the *a priori* XC(0) potential energy surface with no free parameters yielded the overall dimensionless deviation of $\overline{dd}_{\rm exp}=90$ (which indicates that on average, the discrepancies with the input data are 90 times their uncertainties). This is similar to the level of disagreement found in Ref. 7 for the analogous *a priori* XC(0) surface for H_2-Ar. Relative to the high quality of the spectroscopic data, this is not a bad level of agreement, especially in view of the relatively modest level of computational effort required for generating a XC-type potential surface.

As the long-range coefficients are mainly determined by the input theoretical $C_n^{(\lambda)}(\xi)$ values, our initial fits varied only the coefficients $\{F_{\lambda,k}\}$ of the corrector function modifying the Heitler–London interaction energy. After some experimentation it was found that use of five $F_{\lambda,k}$ expansion parameters, three for $\lambda=0$ and two for $\lambda=2$, gave a fairly good fit, and this parametrization was used for $\mathfrak{F}$ in the later stages of this work.

The orders of the polynomials in ξ used to represent the various long-range $C_n^{(\lambda)}(\xi)$ coefficients of Eq. (7) (see Table V) were determined from independent fits to the theoretical values alone. Note that for $\lambda>0$, one of these expansion coefficients is defined in terms of the others using the collapsed diatom limit constraint of Eq. (8). The absence of data involving vibrationally excited $n_v=1$ van der Waals bond stretching level (which lies very close to dissociation) means that the H_2-Kr IR data are relatively less sensitive to the long-range potential coefficients than was the case for H_2-Ar. This was demonstrated by the fact that when all of the $\{C_n^{\lambda,k}\}$ coefficients and $\{F_{\lambda,k}\}$ parameters were allowed to vary simultaneously, the fit failed to converge because of excessive interparameter correlation. As a result, only the coefficients $\{C_n^{\lambda,k}\}$ for $\lambda=0$ and $n=6$, 8, and 10 were allowed to vary independently in the global fits, while those for $\lambda=2$ were fitted using the group scaling parameters $Q_n^{(2)}$ of Eq. (10). The coefficients for $\lambda\geqslant 4$ and $(n,\lambda)=(12,0)$ were fixed at rounded values based on the fit to the *ab initio* $C_n^{(\lambda)}(\xi)$ values alone (i.e., $Q_8^{(4)}=Q_{10}^{(4)}=Q_{10}^{(6)}=Q_{12}^{(0)}=1$).

The values of the 19 fitted parameters defining our final recommended H_2-Kr potential energy surface, with their 95% confidence limit uncertainties given in parentheses, are listed in Table V, together with the fixed $\{C_n^{\lambda,k}=C_{n,\rm th}^{\lambda,k}\}$ coefficients for $\lambda\geqslant 2$ (values with no uncertainties shown); the requisite $R_m^{(\lambda)}$ expansion parameters of Eq. (4) and $E_{\rm HL}^{(1)}$ expansion parameters of Eq. (3) are listed in Table I. When combined with the dispersion energy damping and corrector

TABLE V. Parameters defining the optimized XC(fit) potential, with their 95% confidence limit uncertainties given in parentheses, where the expansion parameters of Eq. (4) are given in Table I.

Heitler–London energy scaling parameters $F_{\lambda,k}$

	$k=0$	$k=1$	$k=2$
$\lambda=0$	1.016 94 (0.0034)	0.083 5 (0.0186)	−0.103 5 (0.038)
$\lambda=2$	−0.055 94 (0.0012)	−0.092 9 (0.0048)	

Long-range expansion coefficients $C_n^{\lambda,k}$ (a.u.)

n	λ	$k=0$	$k=1$	$k=2$	$k=3$	$k=4$
6	0	39.293 (0.178)	34.695 (0.83)	1.6 (0.51)	−8.05 (0.95)	
6	2	3.828 83	8.254 6	3.662	−2.402 3	−1.638 53
8	0	977.21 (18)	1 119.2 (81)	313.87 (55)	−143.2 (100)	
8	2	215.6	624.3	603.	194.3	
8	4	11.124	41.15	44.7	14.674	
10	0	29 437. (1 290)	42 730. (3 970)	22 617. (3 890)		
10	2	7 491.	24 260.	28 450.	11 681.	
10	4	470.2	2 380.	4 250.	2 340.2	
10	6	39.3	145.	232.	126.3	
12	0	1 063 800.	1 410 000.	581 000.		

Long-range group scaling parameters $Q_n^{(2)}$	$n=6$	$n=8$	$n=10$
$[Q_n^{(\lambda)} \equiv 1$ for $\lambda \geq 4$ and $n=12]$	1.0009 (0.0043)	1.114 (0.036)	1.153 (0.064)

functions of Table II they provide a complete description of our final recommended three-dimensional potential energy surface for the H_2-Kr system. While this final function has a rather cluttered analytic form, a FORTRAN subroutine for generating it may be obtained either from the authors[91] or from the Journal's online archive.[70] Note that except for some of the leading $C_n^{\lambda,k}$ coefficients, most of the fitting parameters have no physical significance. However, the quality of the theoretical $C_n^{(\lambda)}(\xi)$ values does lead us to expect that the $\{Q_n^{(\lambda)}\}$ scaling parameters should be close to unity and that the value of $\overline{dd}_{\text{th}}$ for the final fit should be $\lesssim 1$. Moreover, the physical reasonableness of the *a priori* XC(0) potential surface leads us to expect that the value of $F_{0,0}$ should be close to unity and that the magnitude of other $F_{\lambda,k}$'s should be small. Tables V and VI show that all of these expectations are satisfied, and the similarity of the $C_n^{(\lambda)}(\xi)$ functions for the XC(0) and XC(fit) potentials (dashed vs solid curves in Fig. 1) confirms the assertion that they are largely determined by the input theoretical values and their uncertainties, and do not have to be modified excessively to yield agreement with the spectroscopic data.

The quality of the fit to the three types of data used in the analysis is indicated by the $\overline{dd}_\gamma$ values listed in the upper segment of Table VI, together with analogous results for the XC(0) surface and for the TT_3 potential of Ref. 6. The agreement with the spectroscopic data is remarkably good, and is particularly impressive when expressed in absolute terms: the discrepancies with the experimental IR transition frequencies are on average only 0.56 times the estimated experimental uncertainties, or 0.0028 cm^{-1}. Comparison with analogous predictions for the *a priori* XC(0) surface shows that our morphing procedure, mainly depending on the five $\{F_{\lambda,k}\}$ parameters of Eq. (11), improved the agreement with the experimental data by a factor of about 160. The factor of

TABLE VI. Dimensionless rms deviations $\overline{dd}_\lambda$ for various properties predicted using the TT_3 potential of Ref. 6, our *a priori* XC(0) potential, and our recommended XC(fit) potential for the H_2-Kr system. The values of $\overline{dd}_{\text{vir}}$ and $\overline{dd}_{\text{dif}}$ were calculated assuming experimental uncertainties of ±5 $cm^3\,mol^{-1}$ and 0.3%, respectively.

	Input data		Potential		
	Number	Reference	TT_3	XC(0)	XC(fit)
Properties used in the fit					
IR data: $\lambda=$ir	219	34	3.72	76.44	0.56
Hyperfine datum: $\lambda=$nf	1	22	3.84	705.5	1.62
Long-range coefficients: $\lambda=$th	74	71	n/a	0.12	0.55
Total: $\lambda=$tot	294	22, 34, and 71	3.72	77.75	0.57
Property not used in the fit					
Virial coefficients: $\lambda=$vir	11	36	0.48	0.40	0.43
Diffusion coefficients: $\lambda=$dif	19	37	4.31	1.42	0.74

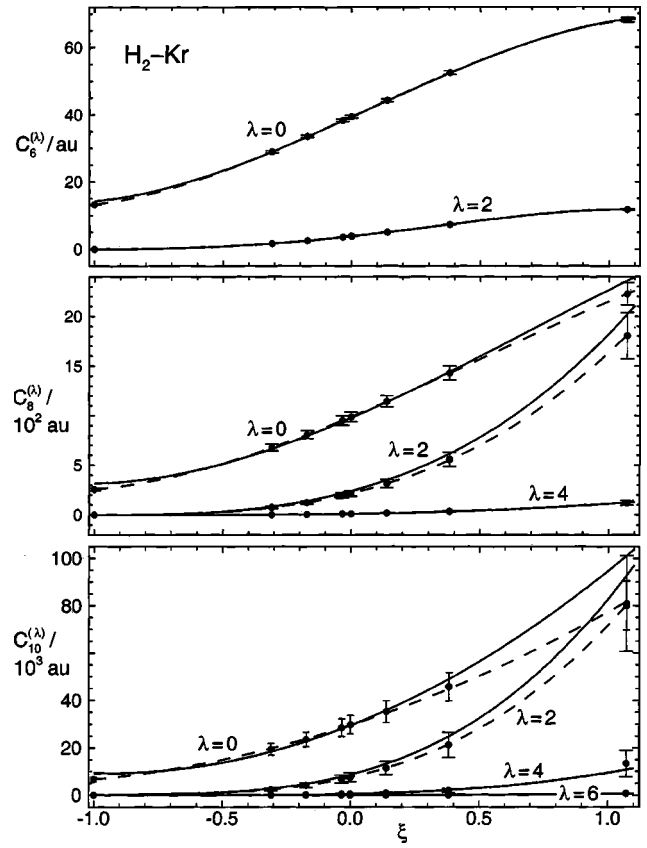

FIG. 1. Long-range stretching-dependent potential energy coefficients $C_n^{(\lambda)}(\xi)$ for H_2-Kr. The input theoretical values (Refs. 71 and 72) and their estimated uncertainties are points with error bars, while the fitted functions associated with the XC(0) and XC(fit) potentials are shown as dashed and solid curves, respectively.

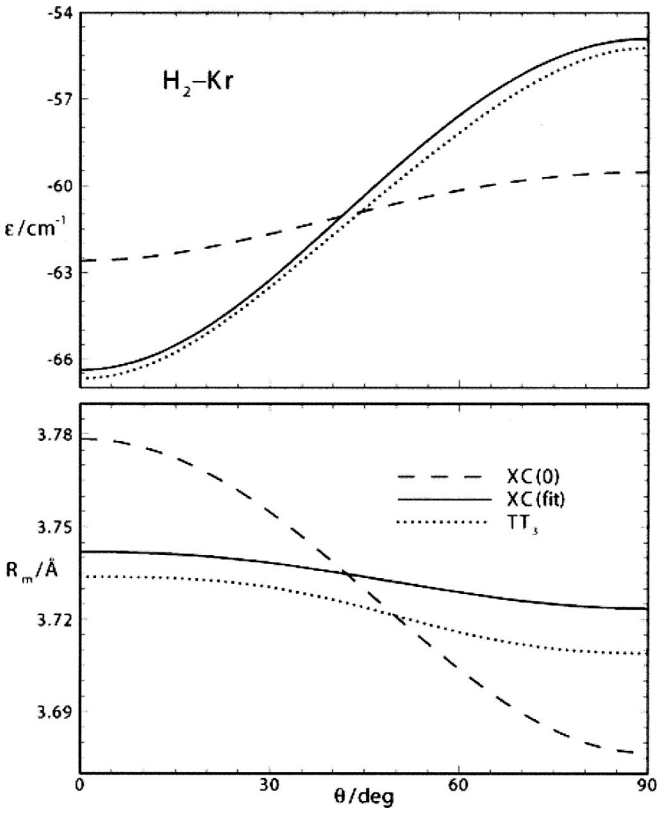

FIG. 2. Dependence of the potential minimum energy (ε) and its radial position (R_m) on θ (at $\xi=0$) for three different H_2-Kr potentials.

7 difference with the quality of predictions generated from the TT_3 surface is consistent with the factor of 5–7 improvement in the precision of the IR data used in our analysis. More detailed comparisons of the predictions of our final recommended surface with the experimental IR data are presented in Ref. 34.

As discussed in Ref. 6, the radio frequency hyperfine transition measured by Waaijer and Reuss[22] depends mainly on the expectation value of the anisotropy strength function $V_{2,0}(R)$ [see Eq. (17)] for levels of H_2-Kr formed from ground state *ortho*-$H_2(v=0,j=1)$. This datum was also included in the data set which determined the TT_3 potential, and that analysis reported a dimensionless discrepancy of only 0.093, a value substantially smaller than the 3.84 shown in Table VI. This difference between the present and previous[6] predictions of this property for the same TT_3 potential energy surface reflects the improved accuracy of the ISE procedure used in the present simulations relative to the SEPT procedure used in Ref. 6. The results in the second row of Table VI show that our XC(fit) potential predicts this datum almost within the estimated experimental uncertainty, while the XC(0) potential does very much worse. The difference between the quality of this agreement also correlates with the degree of similarity of the two anisotropy strength functions $V_{2,0}(R)$ in the attractive region (see below).

Figure 1 compares the input *ab initio* values of $C_n^{(\lambda)}(\xi)$ and their estimated uncertainties (from Table III, points and error bars) with the fitted functions associated with the XC(0) (dashed curves) and XC(fit) (solid curves) potentials. These two types of curves are of course identical for $\lambda \geqslant 4$, because the associated $Q_n^{(\lambda)}$ values are fixed at unity. Fitting to the experimental data clearly has only modest effects on the functions representing the $C_n^{(\lambda)}(\xi)$ values, and the agreement with the input values is generally well within the estimated uncertainties. For $C_{10}^{(0)}(\xi)$ this is markedly different than the situation for H_2-Ar, for which we were left with very large relative discrepancies.[7] This improvement is almost certainly due to the fact that an estimate of the higher-order $C_{12}^{(0)}(\xi)/R^{12}$ term generated from Eq. (9) was included in the potential function model used here.

B. Comparisons, testing, and predictions of the new potential

Figures 2–4 compare features of our recommended XC (fit) potential with those of our *a priori* XC(0) surface and the TT_3 potential of Ref. 6. In particular, Fig. 2 shows how the position R_m and depth ε of the radial minimum varies with relative orientation when the H_2 stretching coordinate is fixed at $\xi=0$. For all three surfaces the global minimum lies at the collinear geometry $\theta=0$ (or π). The XC(fit) and TT_3 surfaces have almost the same energy minima, with depths differing by only $\sim 0.5\%$ and minimum positions by only $\sim 0.2\%-0.4\%$; for the *a priori* XC(0) surface the analogous discrepancies are 6%–8% and 1%, respectively. The well depth of the *a priori* XC(0) potential clearly changes dis-

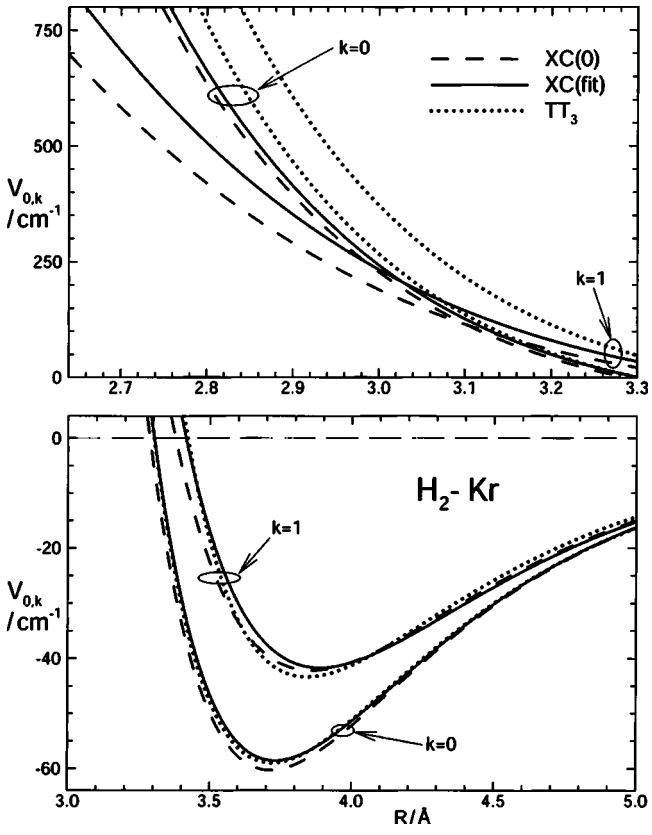

FIG. 3. Radial strength functions $V_{0,0}(R)$ and $V_{0,1}(R)$ of Eq. (17) for three different H_2-Kr potentials.

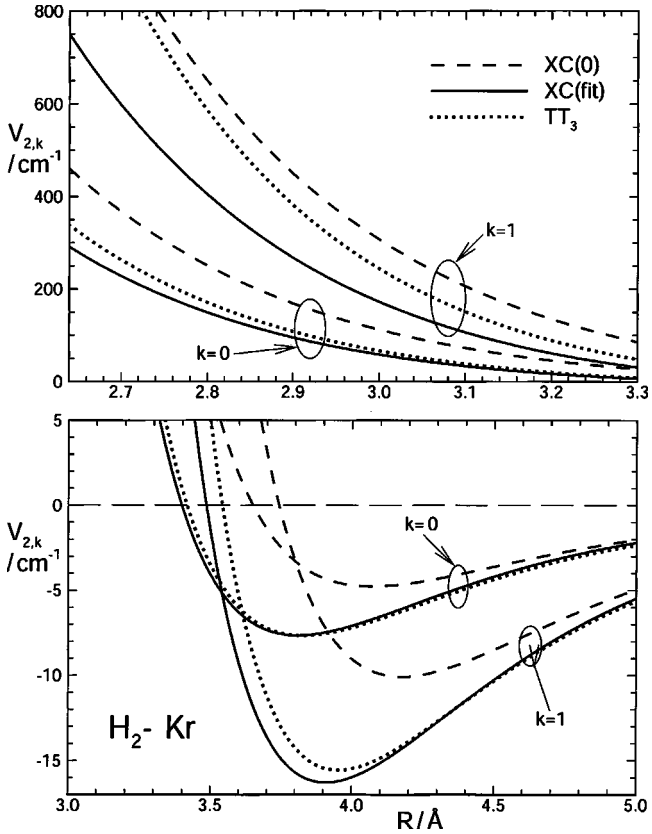

FIG. 4. Radial strength functions $V_{2,0}(R)$ and $V_{2,1}(R)$ of Eq. (17) for three different H_2-Kr potentials.

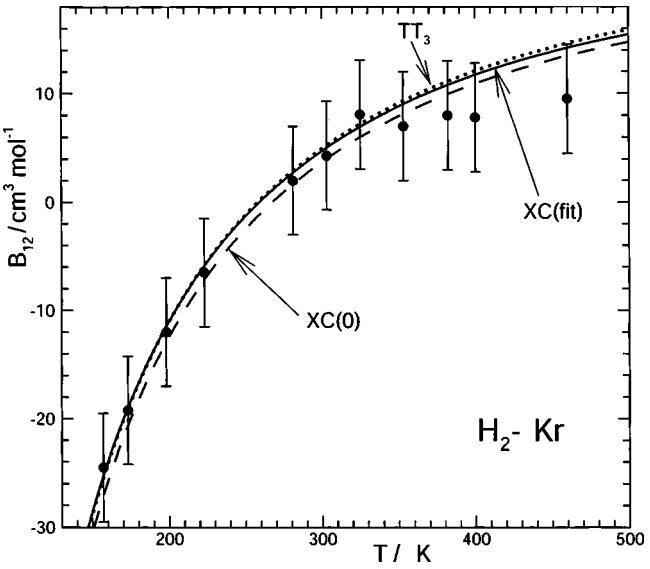

FIG. 5. Interaction virial coefficients for H_2-Kr (in units $cm^3\,mol^{-1}$) calculated from the XC(fit) (solid curve), XC(0) (dashed curve), and TT_3 (dotted curve) potentials, compared with experimental data from Ref. 36.

tinctly too little with θ, while its minimum position varies too much. This is the same qualitative weakness found for the XC(0) potential of H_2-Ar,[7] but again, the empirical scaling introduced by the $\mathcal{F}$ function sufficed to yield a fully satisfactory surface.

A more conventional way of comparing potentials involves examining the radial strength functions $V_{\lambda,k}(R)$ defined by the expansions of Eq. (17): for the three surfaces of interest, the four leading terms of this expansion are compared in Figs. 3 and 4. Figure 3 shows the basic isotropic potentials $V_{0,0}(R)$ and the radial functions $V_{0,1}(R)$ defining their linear stretching dependence, while Fig. 4 shows the analogous functions defining the strength of the $P_2(\cos\theta)$ anisotropy, $V_{2,0}(R)$, and its linear stretching dependence $V_{2,1}(R)$. In spite of the marked differences among the anisotropy strength functions seen in Fig. 4, it is interesting to note (see Fig. 3) that the isotropic part of the XC(0) potential and its linear ξ dependence are both quite similar to the analogous components of the optimized XC(fit) surface. In any case, it is clear that the basic isotropic potential $V_{0,0}(R)$ is remarkably similar for all three potentials, but there are significant differences among the other components. In contrast, the magnitude of $\overline{dd}_{ir}$ for the XC(0) potential (see Table VI) reflects the substantial differences between its basic ($k=0$) anisotropy strength function in the well region and those of the other potentials (see the lower segment of Fig. 4).

The lower segment of Table VI and Figs. 5 and 6 compare the ability of the TT_3, XC(0), and XC(fit) potential energy surfaces to predict values of two properties which were not used in the determination of the XC(fit) potential, interaction virial coefficients[36] and diffusion coefficients.[37] For both properties, the results shown were obtained from exact quantum calculations[92,93] using the isotropic, rigid-diatom version of the indicated potential, as obtained by averaging over the diatom stretching coordinate for the specified vibration-rotation level to give $\overline{V}_{v,j}(R,\theta) = \langle v,j|V(R,\theta,r)|v,j\rangle$, and then projecting out the isotropic

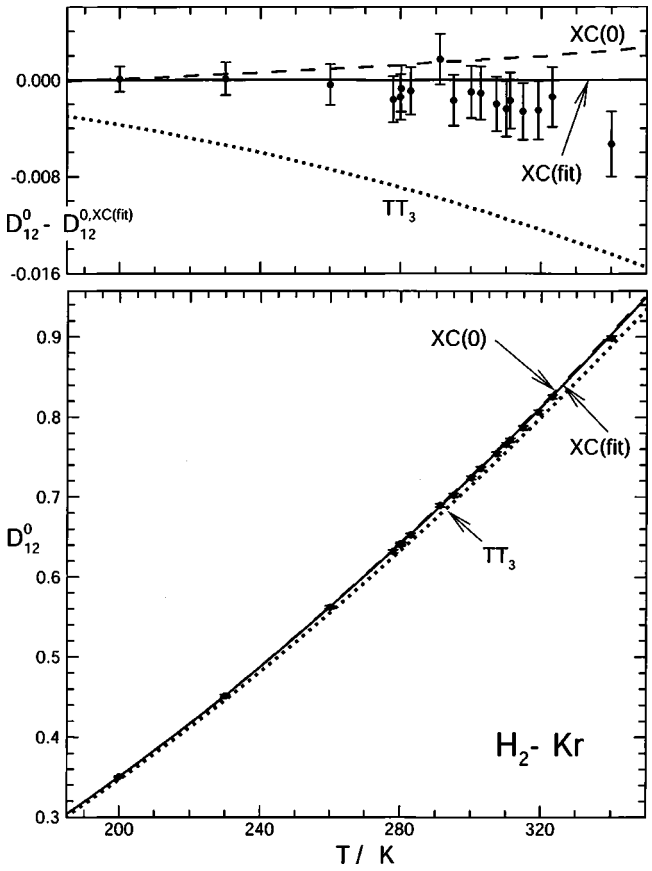

FIG. 6. Lower: Diffusion coefficients for H_2 in Kr (in units $cm^2\ s^{-1}$) calculated from the XC(fit) (solid curve), XC(0) (dashed curve), and TT_3 (dotted curve) potentials, compared with experimental data from Ref. 37. Upper: Diffusion coefficients for H_2 in Kr, as below, relative to values calculated from the XC(fit) potential.

component $\overline{V}^{\rm eff}_{v,j}(R)=\langle Y_{0,0}|\overline{V}_{v,j}(R,\theta)|Y_{0,0}\rangle$. For the interaction virial coefficients, additional tests included performing fully classical and semiclassical (i.e., classical plus first quantum correction) calculations[94,95] using the vibrationally averaged anisotropic potentials $\overline{V}_{v,j}(R,\theta)$. While the predictions of the pure classical calculation were slightly different, the semiclassical calculation using the two-dimensional anisotropic potential yielded results essentially identical to those obtained from the quantal calculation on the isotropic potential. We therefore concluded that the latter provide a very accurate description of this property in the temperature range considered.

Since second virial coefficients are known to be mainly dependent on the effective isotropic radial potential energy well, it is not surprising that the various calculated values of $\overline{dd}_{\rm vir}$ seen in Table VI are all fairly similar. This (expected) inability to distinguish among different potential surfaces is one reason that those data were not included in the least-squares analysis to determine our H_2-Kr potential.

In contrast with the interaction virial coefficients, the diffusion coefficients show a very distinct preference for the XC(fit) potential, a preference most clearly illustrated by the difference plot in the upper segment of Fig. 6. While it is gratifying to see the excellent level of agreement found for the XC(fit) potential, in view of the results in the upper segment of Table VI it is, perhaps, somewhat surprising that the predictions yielded by the TT_3 potential are much worse than those for the XC(0) potential. However, diffusion coefficients mainly depend on the isotropic average of the repulsive wall of the potential. The upper segment of Fig. 3 shows that the TT_3 curve deviates from the XC(fit) potential in that region much more than does the XC(0) potential, and the direction and relative magnitude of those differences appear to be directly illustrated by the upper segment of Fig. 6. Table VII presents values of the interaction virial coefficients and diffusion coefficients for H_2-Kr and D_2-Kr systems calculated from our recommended XC(fit) potential energy surface assuming "normal" (i.e., corresponding to the high temperature equilibrium) abundance of *ortho*- and *para*-H_2 or *ortho*- and *para*-D_2. The results for the individual *ortho* and *para* species differ very slightly because of the small differences in the associated vibrationally averaged potentials $\overline{V}^{\rm eff}_{v,j}(R)$. It is interesting to note (see Table VI) that the XC(0) potential, which has no adjustable parameters, yields diffusion and second virial coefficients which are almost in full agreement with experiment.

Finally, Table VIII lists the energies and tunneling predissociation widths (in square brackets) of all bound and quasibound levels of complexes formed from ground-state *para*-H_2 and *ortho*-D_2, as predicted from our recommended XC(fit) surface. Analogous results for complexes formed by Kr with *ortho*-H_2 or *para*-D_2 are presented in the Journal's

TABLE VII. Predicted second interactive virial coefficients B_{12}, diffusion coefficients $\mathcal{D}^0_{12}$, and dimer formation equilibrium constants K_P (for standard state pressure of 1 bar) calculated using the XC(fit) potential of Table V assuming frozen "normal" relative abundances of *ortho*- and *para*-H_2 and D_2 and the average atomic mass for Kr.

	B_{12} ($cm^3\ mol^{-1}$)		$\mathcal{D}^0_{12}$ ($cm^2\ s^{-1}$)		ln (K_P)	
T (K)	H_2-Kr	D_2-Kr	H_2-Kr	D_2-Kr	H_2-Kr	D_2-Kr
77	−109.367	−112.531	0.0561	0.0402	−3.522	−3.501
90	−82.951	−85.057	0.0766	0.0548	−3.953	−3.920
100	−68.295	−69.911	0.0943	0.0675	−4.231	−4.199
120	−47.632	−48.672	0.1346	0.0961	−4.730	−4.679
140	−33.824	−34.552	0.1806	0.1290	−5.143	−5.080
160	−23.988	−24.529	0.2322	0.1658	−5.488	−5.426
180	−16.654	−17.074	0.2889	0.2063	−5.791	−5.729
200	−10.996	−11.332	0.3504	0.2503	−6.061	−5.999
220	−6.511	−6.788	0.4166	0.2977	−6.305	−6.243
240	−2.881	−3.114	0.4873	0.3482	−6.527	−6.465
260	0.110	−0.090	0.5623	0.4019	−6.731	−6.669
280	2.609	2.435	0.6415	0.4586	−6.919	−6.858
300	4.724	4.571	0.7248	0.5182	−7.094	−7.033
320	6.532	6.396	0.8121	0.5808	−7.258	−7.197
340	8.092	7.969	0.9033	0.6461	−7.412	−7.351
360	9.449	9.337	0.9984	0.7141	−7.557	−7.495
380	10.636	10.534	1.0972	0.7849	−7.694	−7.632
400	11.683	11.588	1.1997	0.8583	−7.823	−7.762
420	12.609	12.521	1.3059	0.9344	−7.947	−7.885
440	13.434	13.351	1.4156	1.0130	−8.064	−8.003
460	14.171	14.093	1.5290	1.0942	−8.176	−8.115
480	14.832	14.759	1.6458	1.1779	−8.284	−8.223
500	15.428	15.358	1.7661	1.2640	−8.387	−8.326

TABLE VIII. Energies of levels of $H_2(v,j)$–^{84}Kr formed from ground state *ortho*- and *para*-H_2 calculated from the recommended XC(fit) potential energy surface, with predicted tunneling widths of metastable levels in square brackets (all in cm^{-1}).

		$E(v,j,n_v,l,J)-E_d(v,j)$	
n_v	$l=J$	$H_2(v=0,\ j=0)$	$D_2(v=0,\ j=0)$
0	0	−28.468	−35.540
	1	−27.426	−34.976
	2	−25.350	−33.850
	3	−22.258	−32.167
	4	−18.176	−29.927
	5	−13.145	−27.143
	6	−7.225	−23.823
	7	−0.510	−19.980
	8	6.803[0.031]	−15.630
	9	14.44[0.79]	−10.792
	10		−5.494
	11		0.228[0.000 00]
	12		6.322[0.000 16]
	13		12.681[0.036]
	14		19.18[0.42]
1	0	−1.653	−8.085
	1	−1.171	−7.693
	2	−0.278	−6.914
	3	0.79[0.36]	−5.759
	4		−4.246
	5		−2.406
	6		−0.288
	7		1.995[0.035]
	8		4.35[0.54]

online archive.[70] As one practical application of these results, Table VII also lists values of the equilibrium constants K_P for the formation of bimers between Kr and H_2 or D_2 in their normal (i.e., high temperature equilibrium) ortho and para abundance

$$H_2 + Kr \leftrightarrows H_2 - Kr \tag{33}$$

calculated using standard quantum statistical mechanics expressions.[96] The bound-state partition function used in these calculations included all quasibound levels for which the tunneling lifetime is longer than the average time between collisions at a total pressure of one bar. It is interesting to note that in spite of the very different densities of states, these equilibrium constants are very similar for the two isotopic species. Similarly, the K_P values for complexes formed with *ortho*- and *para*-H_2 differed only by between 3% and 1% from the lowest to highest of the temperatures considered, while for *para*- and *ortho*-D_2 the analogous differences ranged from 0.05% to 0.006%.

VI. SUMMARY AND CONCLUSIONS

This paper describes the determination of a reliable three-dimensional potential energy surface for the H_2-Kr system, which represents the new high resolution IR data for the H_2 and D_2 isotopomers within the experimental uncertainties. This potential surface is based on the XC potential model[7,11,38–43,45–47] which proved to be sufficiently realistic and flexible that only five truly independent empirical parameters are required in the least-squares fits to optimize agreement with the experimental data; these are the $F_{\lambda,k}$ values listed in Table V. This contrasts with the eight parameters (plus additional intuitively justified constraints) required to define the best previous potential for this system.[6] The realistic nature of the components of the basic XC model ensures that this surface should extrapolate well into regions not directly sampled by the experimental data used in the determination of the potential energy surface. This is confirmed by the quality of its predictions of interaction virial coefficients and diffusion coefficients, data which were not used in the analysis. While the present potential has a somewhat complex form, its availability as a documented FORTRAN subroutine should facilitate its use.[70,91,97]

It is also noteworthy that within the average experimental uncertainties of 0.004 cm^{-1}, the 143 IR transitions for H_2-Kr and 76 for D_2-Kr are fully accounted for by the same three-dimensional potential energy surface. In other words, within this resolution the differences between the IR spectra of these isotopomers are fully accounted for by ordinary vibrational averaging (over ξ) and mass considerations, so no Born–Oppenheimer breakdown effects are evident.

The spectroscopic simulations required by the present analysis used the ISE method, which is more accurate than the SEPT procedure used in previous work on this family of systems. The extension of the ISE method described herein allowed the efficient calculation of exact derivatives of level energies with respect to potential energy function parameters, an approach which is more accurate and much more cost effective than the derivative-by-differences approach used heretofore.

It is also appropriate to comment on the choice of the functional form used for the XC potential, as summarized by Eqs. (1)–(11), especially in regard to its diatom bond-stretching or ξ dependence. As indicated by Eq. (17), the XC potential may be expressed as a finite power series in ξ. For the homonuclear H_2 isotopomers, the ξ dependence of the potential may therefore be fully taken into account in quantal close-coupling calculations by simply replacing ξ^k by appropriate expectation values and matrix elements $\langle v',j'|\xi^k|v'',j''\rangle$ for various hydrogen isotopomers, quantities which are readily available[63] and/or readily calculated.[81] While not essential, maintaining this simple linear dependence on matrix elements of powers of ξ is one reason for *not* allowing the scaling distance R_s [see Eq. (4) and discussion below Eq. (6)] to be a function of ξ. For systems involving heteronuclear hydrogen isotopologues (HD, HT, or DT) the situation is somewhat more complicated, but the treatment is still a fairly straightforward procedure. Some details regarding how this is done are included in the comments about our potential function subroutine presented in the Appendix, while more details may be found in Ref. 97.

The fact that the angle dependence of the potential is built into the Heitler–London exponent and damping function scaling distance $R_s=R_m(\theta,\xi=0)$ means that expanding the $V_k(R,\theta)$ functions in terms of the familiar $V_{\lambda,k}(R)$ functions of Eq. (17) requires the use of numerical quadrature

techniques.[98] However, this is true for most other sophisticated potential forms and imposes no significant difficulties. Note that the two-dimensional vibrationally averaged potential for ground-state H_2 is not simply the leading term in the first expansion in Eq. (17), $V_0(R,\theta)$, since expectation values of higher powers of ξ are not zero for H_2 $(v=0, j=0)$.

In conclusion, therefore, we believe that the most productive means of developing realistic and flexible multidimensional potential energy surface models for van der Waals interactions is the type of approach used here. The component Heitler–London and Coulomb interaction energies are relatively easy to calculate, and even without adjustment give a reasonable approximation to the final optimized isotropic surface. The fact that they build in very realistic descriptions of the shapes of and interactions between the component species also means that relatively few empirical parameters are required to refine such models to yield state-of-the-art potentials.

APPENDIX: POTENTIAL FUNCTION SUBROUTINE XCfitH2Kr

Dynamical calculations for an atom-diatom system are generally either classical, simply requiring values of the potential energy function itself for a particular system configuration, or quantum-mechanical coupled-channel calculations which require diagonal and off-diagonal radial channel potential functions associated with various combinations of exit channel diatom vibration-rotational levels. Consideration of the polynomial orders associated with the parametrization of Tables I and V shows that for our XC(fit) potential for H_2–Kr [see Eq. (17)] $k_{\max}=5$:

$$V(R,\theta,\xi)=\sum_{k=0}^{5}\xi^k V_k(R,\theta). \tag{A1}$$

The radial channel potentials required by coupled-channel calculations[4,99] may be generated readily from the expression

$$V_{v,j}^{v',j'}(R,\theta)\equiv\langle v',j'|V(R,\theta,\xi)|v,j\rangle=\sum_{k=0}^{5}\langle\xi^k\rangle_{v,j}^{v',j'}V_k(R,\theta) \tag{A2}$$

in which the requisite diagonal and off-diagonal matrix elements of powers of the diatom stretching coordinate $\langle\xi^k\rangle_{v,j}^{v',j'}\equiv\langle v',j'|\xi^k|v,j\rangle$ may be generated readily from the accurately known potential functions for all isotopologues of ground-state molecular hydrogen[63,91] using standard methods.[81] To facilitate this type of application, our XC(fit) potential energy subroutine XCfitH2Kr offers the option of either having the subroutine return the value of the potential energy function itself for a particular system configuration (R,θ,ξ) or, if an appropriate set of $\langle\xi^k\rangle_{v,j}^{v',j'}$ matrix elements is supplied, returning values of the vibrationally averaged radial channel functions of Eq. (A2).[70,91] However, this straightforward approach would only be valid for interactions involving the homonuclear isotopologs of diatomic hydrogen for which the diatom center of mass is located at the bond midpoint about which our XC(fit) potential is expanded.

Dynamical calculations require the potential energy or radial channel potential functions to be defined in terms of the center-of-mass Jacobi coordinates $(R_{\text{c.m.}},\theta_{\text{c.m.}})$, and for heteronuclear hydrogen they differ significantly from the "bond-midpoint coordinates" $(R_{\text{mid}},\theta_{\text{mid}})$ in terms of which our XC(fit) potential is defined. For a classical calculation which simply requires values of the potential energy at each instantaneous system configuration $(R_{\text{c.m.}},\theta_{\text{c.m.}},\xi)$ this presents little difficulty, since for any such system configuration the associated bond-midpoint coordinate values may readily be generated from the expressions[98]

$$R_{\text{mid}}=R_{\text{c.m.}}[1+2(\delta/R_{\text{c.m.}})\cos\theta_{\text{c.m.}}+(\delta/R_{\text{c.m.}})^2]^{1/2}, \tag{A3}$$

$$\cos\theta_{\text{mid}}=(R_{\text{c.m.}}\cos\theta_{\text{c.m.}}+\delta)/R_{\text{mid}} \tag{A4}$$

in which the distance from the diatom center-of-mass to the bond-midpoint is

$$\delta=-\frac{|M_1-M_2|}{2(M_1+M_2)}r_0(\xi+1) \tag{A5}$$

and M_1 and M_2 are the masses of the atoms forming the hydrogen diatom. If its input parameters indicate that $M_1\neq M_2$, subroutine XCfitH2Kr uses Eqs. (A3)–(A5) to generate the corresponding bond-midpoint coordinate values, and the potential function value is then generated from Eq. (A1) in the usual manner.

For quantum coupled-channel calculations involving heteronuclear hydrogen the situation is somewhat more complicated,[4,98,99] since the coordinate transformation of Eqs. (A3)–(A5) must be applied *before* any diatom vibrational averaging is done. However, Ref. 98 showed that the introduction of an orthogonal polynomial representation for the ξ dependence of the potential energy function greatly simplifies the problem of generating the vibrationally averaged functions required for such cases. For any particular system geometry, the value of the potential energy function is of course the same, no matter which coordinate system is used. As a result, with the center-of-mass and bond-midpoint coordinates related by Eqs. (A3)–(A5), we can write

$$U(R_{\text{c.m.}},\theta_{\text{c.m.}},\xi)=V(R_{\text{mid}},\theta_{\text{mid}},\xi)=\sum_{k=0}^{k'_{\max}}\xi^k U_k(R_{\text{c.m.}},\theta_{\text{c.m.}}) \tag{A6}$$

in which $k'_{\max}\geqslant k_{\max}=5$, and values of the expansion functions $U_k(R_{\text{c.m.}},\theta_{\text{c.m.}})$ are determined from an orthogonal polynomial quadrature procedure.[97] This allows radial channel functions for heteronuclear isotopologs to be generated in the same manner as for homonuclear hydrogen

$$U_{v,j}^{v',j'}(R_{\text{c.m.}},\theta_{\text{c.m.}})\equiv\langle v',j'|U(R_{\text{c.m.}},\theta_{\text{c.m.}},\xi)|v,j\rangle=\sum_{k=0}^{k'_{\max}}\langle\xi^k\rangle_{v,j}^{v',j'}U_k(R_{\text{c.m.}},\theta_{\text{c.m.}}). \tag{A7}$$

Numerical tests show that across the domain $\xi\in[-0.9,+0.9]$, which extends far beyond the region for which our XC(fit) surface is expected to be reliable, for $k'_{\max}=8$ this approach yields transformed potential function values for

HT–Kr (for which $\delta/r=0.2495$) with an accuracy of better than 10^{-4} cm^{-1} in the potential well and low-energy repulsive wall regions, which is two orders of magnitude more precise than the potential function itself.[97] This procedure is implemented in subroutine XCfitH2Kr and is applied automatically in cases for which $M_1 \neq M_2$ and the user requests vibrationally averaged function values of the form of Eq. (A7). For further details, see Ref. 97.

[1]R. J. Le Roy and J. van Kranendonk, J. Chem. Phys. **61**, 4750 (1974).
[2]R. J. Le Roy, J. S. Carley, and J. E. Grabenstetter, Faraday Discuss. Chem. Soc. **62**, 169 (1977).
[3]J. S. Carley, Faraday Discuss. Chem. Soc. **62**, 303 (1977).
[4]R. J. Le Roy and J. S. Carley, in *Potential Energy Surfaces*, Advance Chemical Physics, Vol. 42, edited by K. Lawley (Wiley, New York, 1980), pp. 353–420.
[5]R. J. Le Roy, in *Resonances in Electron-Molecule Scattering, Van der Waals Complexes, and Reactive Chemical Dynamics*, edited by D. Truhlar (American Chemical Society, Washington, DC, 1984), Vol. 263, Chap. 13, pp. 231–262.
[6]R. J. Le Roy and J. M. Hutson, J. Chem. Phys. **86**, 837 (1987).
[7]C. Bissonnette, C. E. Chuaqui, K. G. Crowell, R. J. Le Roy, R. J. Wheatley, and W. J. Meath, J. Chem. Phys. **105**, 2639 (1996).
[8]J. M. Hutson, J. Chem. Phys. **96**, 6752 (1992).
[9]J. M. Hutson, J. Phys. Chem. **96**, 4237 (1992).
[10]C. E. Chuaqui, R. J. Le Roy, and A. R. W. McKellar, J. Chem. Phys. **101**, 39 (1994).
[11]R. J. Le Roy, C. Bissonnette, T. H. Wu, A. K. Dham, and W. J. Meath, Faraday Discuss. **97**, 81 (1994).
[12]A. K. Dham and W. J. Meath, Mol. Phys. **88**, 339 (1996).
[13]M. Thachuk, C. E. Chuaqui, and R. J. Le Roy, J. Chem. Phys. **105**, 4005 (1996).
[14]J. M. Hutson, A. Ernesti, M. M. Law, C. F. Roche, and R. J. Wheatley, J. Chem. Phys. **105**, 9130 (1996).
[15]M. Meuwly and J. M. Hutson, J. Chem. Phys. **110**, 8338 (1999).
[16]M. Quack and M. A. Sum, J. Chem. Phys. **95**, 28 (1991).
[17]M. J. Elrod and R. J. Saykally, J. Chem. Phys. **103**, 933 (1995).
[18]H. L. Williams, K. Szalewicz, B. Jeziorski, R. Moszynski, and S. Rybak, J. Chem. Phys. **98**, 1279 (1993).
[19]R. Moszynski, B. Jeziorski, P. E. S. Wormer, and A. van der Avoird, Chem. Phys. Lett. **221**, 161 (1994).
[20]R. Moszynski, T. Korona, P. E. S. Wormer, and A. van der Avoird, J. Chem. Phys. **103**, 321 (1995).
[21]A. R. W. McKellar and H. L. Welsh, J. Chem. Phys. **55**, 595 (1971).
[22]M. Waaijer and J. Reuss, Chem. Phys. **63**, 263 (1981).
[23]A. R. W. McKellar, Faraday Discuss. Chem. Soc. **73**, 89 (1982).
[24]A. R. W. McKellar, J. Chem. Phys. **105**, 2628 (1996).
[25]A. M. Rulis, K. M. Smith, and G. Scoles, Can. J. Phys. **56**, 753 (1978).
[26]J. P. Toennies, W. Welz, and G. Wolf, J. Chem. Phys. **71**, 614 (1979).
[27]U. Buck, Faraday Discuss. Chem. Soc. **73**, 187 (1982).
[28]U. Buck, H. Meyer, and R. J. Le Roy, J. Chem. Phys. **80**, 5589 (1984).
[29]J. Brewer and G. W. Vaughn, J. Chem. Phys. **50**, 2960 (1969).
[30]B. Schramm, E. Elias, and R. Pilger, Chem. Phys. Lett. **88**, 459 (1982).
[31]P. Lallemand and P. Simova, J. Mol. Spectrosc. **26**, 262 (1968).
[32]R. L. Farrow, L. A. Rahn, G. O. Sitz, and G. J. Rosasco, Phys. Rev. Lett. **63**, 746 (1989).
[33]J. Ph. Berger, R. Saint-Loup, H. Berger, J. Bonamy, and D. Robert, Phys. Rev. A **49**, 3396 (1994).
[34]A. R. W. McKellar, J. Chem. Phys. **122**, 084320 (2005), preceding paper.
[35]J. S. Carley, Ph.D. thesis, University of Waterloo, Waterloo, 1978.
[36]S. Pérez, H. Schmiedel, and B. Schramm, Z. Phys. Chem., Neue Folge **123**, 35 (1980).
[37]P. J. Dunlop, H. L. Robjohns, and C. M. Bignell, J. Chem. Phys. **86**, 2922 (1987); R. D. Trengove and P. J. Dunlop, Ber. Bunsenges. Phys. Chem. **87**, 874 (1983).
[38]K.-C. Ng, W. J. Meath, and A. R. Allnatt, Chem. Phys. **32**, 175 (1978).
[39]K.-C. Ng, W. J. Meath, and A. R. Allnatt, Mol. Phys. **37**, 237 (1979).
[40]W. J. Meath, D. J. Margoliash, B. L. Jhanwar, A. Koide, and G. D. Zeiss, in *Proceedings of the 14th Jerusalem Symposium on Quantum Chemistry, and Biochemistry*, edited by B. Pullman (Reidel, Dordrecht, 1981), pp. 101–115.
[41]A. K. Dham, A. R. Allnatt, W. J. Meath, and R. A. Aziz, Mol. Phys. **67**, 1291 (1989).
[42]A. K. Dham, W. J. Meath, A. R. Allnatt, R. A. Aziz, and M. J. Slaman, Chem. Phys. **142**, 173 (1990).
[43]W. J. Meath and M. Koulis, J. Mol. Struct.: THEOCHEM **226**, 1 (1991).
[44]R. A. Aziz, M. J. Slaman, A. Koide, A. R. Allnatt, and W. J. Meath, Mol. Phys. **77**, 321 (1992).
[45]A. Dham and W. J. Meath, Chem. Phys. **196**, 125 (1995).
[46]A. K. Dham, F. R. W. McCourt, and W. J. Meath, J. Chem. Phys. **103**, 8477 (1995).
[47]A. K. Dham and W. J. Meath, Mol. Phys. **99**, 991 (2001).
[48]R. Wheatley, A. S. Tulegenov, and E. Bichoutskaia, Int. Rev. Phys. Chem. **23**, 151 (2004).
[49]J. Hepburn, G. Scoles, and R. Penco, Chem. Phys. Lett. **36**, 451 (1975).
[50]R. Ahlrichs, R. Penco, and G. Scoles, Chem. Phys. **19**, 119 (1977).
[51]C. Douketis, G. Scoles, S. Marchetti, M. Zen, and A. J. Thakkar, J. Chem. Phys. **76**, 3057 (1982).
[52]W. R. Rodwell and G. Scoles, J. Phys. Chem. **86**, 1053 (1982).
[53]F. R. W. McCourt, F. B. van Duijneveldt, T. van Dam, and R. R. Fuchs, Mol. Phys. **61**, 109 (1987).
[54]K. T. Tang and J. P. Toennies, J. Chem. Phys. **66**, 1496 (1977).
[55]K. T. Tang and J. P. Toennies, J. Chem. Phys. **68**, 5501 (1978).
[56]K. T. Tang and J. P. Toennies, J. Chem. Phys. **76**, 2524 (1982).
[57]K. T. Tang and J. P. Toennies, J. Chem. Phys. **80**, 3726 (1984).
[58]M. S. Bowers, K. T. Tang, and J. P. Toennies, J. Chem. Phys. **88**, 5465 (1988).
[59]J. M. Hutson and R. J. Le Roy, J. Chem. Phys. **83**, 1197 (1985).
[60]T. Slee and R. J. Le Roy, J. Chem. Phys. **99**, 360 (1993).
[61]T. Slee, R. J. Le Roy, and C. E. Chuaqui, Mol. Phys. **77**, 111 (1992).
[62]H. Kreek and W. J. Meath, J. Chem. Phys. **50**, 2289 (1969).
[63]C. Schwartz and R. J. Le Roy, J. Mol. Spectrosc. **121**, 420 (1987).
[64]H. Kreek and W. J. Meath, J. Chem. Phys. **50**, 2289 (1969).
[65]A. Koide, W. J. Meath, and A. R. Allnatt, Chem. Phys. **58**, 105 (1981).
[66]R. D. Amos and J. E. Rice, CADPAC—The Cambridge Analytic Derivatives Package, Issue 4.0, 1987.
[67]I. C. Hayes and A. J. Stone, Mol. Phys. **53**, 69 (1984); **53**, 83 (1984).
[68]R. J. Wheatley and W. J. Meath, Mol. Phys. **79**, 253 (1993).
[69]B. H. Wells, Mol. Phys. **61**, 1283 (1987).
[70]See EPAPS Document No. E-JCPSA6-122-007507 for ASCII files containing a listing of the *ab initio* Heitler–London enegies obtained here, a listing of all possible IR transitions predicted from the recommended XC(fit) potential surface, a list of calculated eigenvalues and tunneling predissociation level widths for all bound and quasibound levels of complexes formed from ground-state *para*- or ortho- H_2 and D_2, and a Fortran subroutine for generating our recommended XC(fit) potential and a manual describing how to use it. A direct link to this document may be found in the online article's HTML reference section. The document may also be reached via the EPAPS homepage (http://www.aip.org/pubservs/epaps.html) or from ftp.aip.org in the directory /epaps/. See the EPAPS homepage for more information.
[71]P. E. S. Wormer, H. Hettema, and A. J. Thakkar, J. Chem. Phys. **98**, 7140 (1993).
[72]W. J. Meath and A. Kumar, Int. J. Quantum Chem., Quantum Chem. Symp. **24**, 501 (1990).
[73]W. Kolos and L. Wolniewicz, J. Chem. Phys. **43**, 2429 (1965).
[74]W. Kolos and L. Wolniewicz, Chem. Phys. Lett. **24**, 457 (1974).
[75]A. Kumar and W. J. Meath, Mol. Phys. **54**, 823 (1985).
[76]J. M. Standard and P. R. Certain, J. Chem. Phys. **83**, 3002 (1985).
[77]T. H. Wu and W. J. Meath, (unpublished).
[78]R. A. Aziz and H. H. Chen, J. Chem. Phys. **67**, 5719 (1977).
[79]A. Koide, W. J. Meath, and A. R. Allnatt, Mol. Phys. **39**, 895 (1980).
[80]J. M. Hutson, BOUND computer code, Version 5 (1993), distributed by Collaborative Computational Project No. 6 of the Science and Engineering Research Council (UK).
[81]R. J. Le Roy, LEVEL 7.5: A Computer Program for Solving the Radial Schrödinger Equation for Bound and Quasibound Levels, University of Waterloo Chemical Physics Research Report No. CP-655, 2002; see the "Computer Programs" link at http://leroy.uwaterloo.ca
[82]J. M. Hutson, in *Advances in Molecular Vibrations and Collision Dynamics*, edited by J. M. Bowman (JAI, Greenwich, CT, 1991), Vol. 1A, Chap. 1, pp. 1–45.

[83]I. C. Percival and M. J. Seaton, Proc. Cambridge Philos. Soc. **53**, 654 (1957).
[84]A. M. Arthurs and A. Dalgarno, Proc. R. Soc. London, Ser. A **256**, 540 (1960).
[85]M. Waaijer, M. Jacobs, and J. Reuss, Chem. Phys. **63**, 247 (1981).
[86]In a zero-coupling limit, the $\phi^a_{n_v}(R)$ functions are simply the eigenfunctions of the effective one-dimensional radial "distortion" potential (Ref. 59) $(\Phi_a^{JM_J}|V(R,\theta,r)|\Phi_a^{JM_J})$.
[87]I. Mills, T. Cvitaš, K. Homann, N. Kallay, and K. Kuchitsu, *Quantities, Units and Symbols in Physical Chemistry*, 2nd ed. (Blackwell Science, Oxford, 1993).
[88]R. J. Le Roy and R. B. Bernstein, J. Chem. Phys. **54**, 5114 (1971).
[89]R. J. Le Roy and W.-K. Liu, J. Chem. Phys. **69**, 3622 (1978).
[90]R. J. Le Roy, J. Mol. Spectrosc. **191**, 223 (1998).
[91]To obtain this material, select the "Potential Functions" link at http://leroy.uwaterloo.ca
[92]S. Y. Larsen and J. D. Poll, Can. J. Phys. **52**, 1914 (1974).
[93]F. R. W. McCourt, J. J. M. Beenakker, W. E. Köhler, and I. Kuščer, *Nonequilibrium Phenomena in Polyatomic Gases* (Clarendon, Oxford, 1990), Vol. 1.
[94]E. A. Mason and T. H. Spurling, *The Virial Equation of State* (Pergamon, Oxford, 1969).
[95]G. C. Maitland, M. Rigby, E. B. Smith, and W. A. Wakeham, *Intermolecular Forces—Their Origin and Determination* (Oxford University Press, Oxford, UK, 1981).
[96]D. A. McQuarrie, *Statistical Thermodynamics* (University Science Books, Mill Valley, CA, 1973).
[97]R. J. Le Roy and H. Wei, FORTRAN Subroutines for Generating XC(fit) Potential Functions for the H_2–(rare gas) Systems, University of Waterloo Chemical Physics Research Report No. CP-659, 2004 (Refs. 70 and 91).
[98]W.-K. Liu, J. E. Grabenstetter, R. J. Le Roy, and F. McCourt, J. Chem. Phys. **68**, 5028 (1978).
[99]W. A. Lester, Jr., in *Dynamics of Molecular Collisions*, Modern Theoretical Chemistry Vol. 1, edited by W. H. Miller (Plenum, London, 1976), Chap. 1, pp. 1–32, Part A.